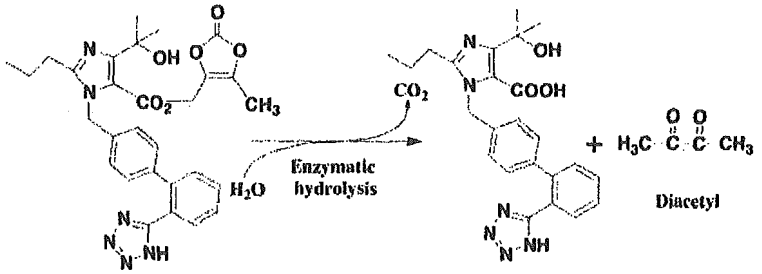

Olmesartan medoxomil CS-866 Ester prodrug

Olmesartan RNH-6270 Active metabolite

FIG. 1. Hydrolysis of CS-866 to RNH-6270

presence and absence of various ligands. Then, we examined the importance of certain types of amino acid residues of HSA for the hydrolysis of CS-866, using chemical modification techniques. Recombinant HSA (rHSA) proteins with alterations of specific amino acid residues were prepared using site-directed mutagenesis techniques, to obtain detailed information about the contribution of those residues. Finally, computer docking models of CS-866 and HSA were constructed and were found to be consistent with the experimental results.

Materials and Methods

Materials. HSA was donated by the Chemo-Sera-Therapeutic Research Institute (Kumamoto, Japan). HSA was defatted before use (Chen, 1967).

CS-866 and RNH-6270 were donated by Sankyo Co., Ltd. (Tokyo, Japan). PNPA, succinic anhydride and *n*-butyl *p*-aminobenzoate (*n*-butyl *p*-AB) were purchased form Nakalai Tesque (Kyoto, Japan). Warfarin was obtained from Eisai Co. (Tokyo, Japan), ibuprofen was obtained from Kaken Pharmaceutical Co. (Osaka, Japan), diazepam was obtained from Sumitomo Pharmaceutical Co. (Osaka, Japan), tetranitromethane was obtained from Aldrich Chemical Co. (Milwaukee, WI), and trinitrobenzenesulfonic acid was obtained from Wako Pure Chemical Industries, Ltd. (Osaka, Japan). Dansyl-L-asparagine (DNSA), 2-hydroxyl-5-nitrobenzyl bromide, and diethyl pyrocarbonate were purchased from Sigma-Aldrich (St. Louis, MO). Restriction enzymes, T4 polynucleotide kinase, calf intestinal alkaline phosphatase, a DNA ligation kit, TaKaRa EX *Taq*DNA polymerase, and a site-directed mutagenesis kit (oligonucleotide-directed dual amber method) were obtained from Takara Shuzo Co., Ltd. (Kyoto, Japan). A DNA sequence kit was obtained from Applied Biosystems (Tokyo, Japan). The *Pichia* Expression kit was purchased from Invitrogen (Carlsbad, CA). All other chemicals were of analytical grade.

Esterase-Like Activity Measurement. *Procedures for Michaelis-Menten Equation Runs.* The reaction was started by adding CS-866 in 100% acetonitrile (5 μl) to preincubated HSA (120 μl, 75 μM), at a final concentration of 10 to 250 μM. Incubation proceeded for 10 min and was terminated by adding 500 μl of acetonitrile to the incubation mixture. We have checked that 4% acetonitrile has little effect on the reaction. After centrifugation for 1 min, a 30-μl aliquot of the deproteinized supernatant was subjected to high-performance liquid chromatography, and RNH-6270 was separated from CS-866 on an ODS column using the following conditions: column, YMC-Pack ODS-AM, AM-302, 150 × 4.6 mm i.d.; column temperature, 40°C maintained by a Hitachi 655A-52 column oven; a Hitachi L-6000 pump; a Hitachi FL detector L-7480 fluorescent monitor; a HITACHI D-2500 Chromato-Integrator; mobile phase, acetonitrile/water/acetic acid, 40:60:0.1; wavelength, excitation = 260 nm, emission = 370 nm; flow rate, 1.0 ml/min.

The reaction between CS-866 and HSA took place at 4°C. Under that condition, Michaelis-Menten equation analysis can be applied.

$$v = \frac{V_{max}[S]}{K_M + [S]} \tag{1}$$

Here, [*S*] is the concentration of substrate. That is the case, because previous studies have revealed a linear relationship between 1/*V* and 1/*S* when plotted in a Lineweaver-Burk plot (Koike et al., 2001):

$$\frac{1}{v} = \frac{1}{V_{max}} + \frac{K_M}{V_{max}[S]} \tag{2}$$

Procedures for Kinetic Runs. Hydrolysis of CS-866 (5 μM) by HSA (at least a 5-fold excess concentration over the substrate) was performed using conditions able to avoid complications due to multiple reactive sites of albumin. Under such conditions, pseudofirst-order rate constant analysis can be performed. The pseudofirst-order rate constant for the release of RNH-6270 (k_{obs}), the dissociation constant of the substrate-HSA complex (K_S), and the catalytic rate constants (k_{cat}) were calculated as reported elsewhere (Sakurai et al., 2004).

Thermodynamic Analysis. Thermodynamic analysis of the HSA-catalyzed reaction was performed at temperatures ranging from 20°C to 40°C. We calculated the thermodynamic parameters, the free energy change for the initial reaction between enzyme and substrate (ΔG_S), the activation free energy for the rate-determining step (ΔG), the free energy difference for the reaction (ΔG_T), the activation energy (E_a), the activation enthalpy change (ΔH), and the activation entropy change (ΔS), using previously published methods (Sakurai et al., 2004).

Effects of Ligands. HSA (120 μl, 75 μM) was preincubated, and the enzymatic reaction was started by adding CS-866 in 100% acetonitrile (5 μl) to the solution, at a final concentration of 100 to 250 μM, in the presence or absence of each ligand (at a final concentration of 0–600 μM) (Ikeda, 2000). Incubation proceeded for 10 min at 37°C, and the release of RNH-6270 was measured by high-performance liquid chromatography as described above.

Chemical Modification of HSA. *Histidine Residues.* Chemical modification of His residues was performed using diethyl pyrocarbonate (Roosemont, 1978). An average of 2.22 His residues was modified out of the total of 16 His residues.

Lysine Residues. Chemical modification of Lys residues was performed according to the method of Gounaris and Perlmann (1967). The modification ratio was calculated as described by Haynes et al. (1967). An average of 3.80 of the 59 Lys residues was modified.

Tyrosine Residues. Chemical modification of Tyr residues was performed as outlined by Sokolovsky et al. (1966). An average of 1.24 of the 18 Tyr residues was modified.

Tryptophan Residues. Chemical modification of the single Trp residue was performed at room temperature (Fehske et al., 1978). An average of 0.88 of the 1 Trp residue was modified.

Chemical modifications of specific amino acid residues (Tyr, Lys, His, and Trp) were performed with the assumption that the effects on other amino acid residues would be negligible. The secondary and tertiary protein structures of all the modified HSAs were examined by circular dichroism measurements before use, and no significant difference was observed between the derivatives and native HSA (data not shown).

Synthesis and Purification of rHSA Forms. The recombinant DNA techniques used to produce wild-type rHSA and the single-residue mutants were

essentially the same as those described by Watanabe et al. (2001). A chimeric plasmid (pJDB-ADH-L10-HSA-A) containing cDNA for the mature form of HSA and an L10 leader sequence was donated by Tonen Co. (Tokyo, Japan). The mutagenic primers used (underlined letters indicate mismatches) were as follows: 5′-CAAACAGAGACTCGCCTGTGCCAGTCTCC-3′ for K199A; 5′-GAGCTTTCAAAGCAGCTGCAGTAGCTCGCCTG-3′ for W214A; 5′-CTATTAGTTCGTGCCACCAAG-3′ for Y411A.

The L10-HSA coding region was amplified by polymerase chain reaction using a forward and a reverse primer containing a 5′-terminal EcoRI site, and was cloned into the EcoRI-digested pKF19k vector (Takara Shuzo Co. Ltd.), and mutagenesis was then performed. The mutation was confirmed by DNA sequencing of the entire HSA coding region using the dideoxy chain termination method and an Applied Biosystems ABI Prism 310 Genetic Analyzer. To construct the HSA expression vector pHIL-D2-HSA, an L10-HSA coding region with or without the desired mutation site was incorporated into the methanol-inducible pHIL-D2 vector (Invitrogen). The resulting vector was introduced into the yeast species *Pichia pastoris* (strain GS115) to express rHSA. Secreted rHSA was isolated from the growth medium by precipitation with 60% ammonium sulfate at room temperature, and was then purified using a column of Blue Sepharose CL-6B (GE Healthcare, Little Chalfant, Buckinghamshire, UK). The eluted rHSA was deionized and then defatted using charcoal treatment.

The resulting protein exhibited a single band on an SDS/polyacrylamide gel, and all of the recombinant proteins migrated to the same position as native HSA (data not shown). Any secondary or tertiary structural differences between native (wild-type) and mutant rHSAs were analyzed by circular dichroism (data not shown). In the far-UV and near-UV regions, all rHSAs exhibited the same characteristics as native HSA.

Docking of CS-866 to HSA. To dock CS-866 to HSA, we used the crystal structure of the HSA-myristate-*S*-warfarin complex (PDB ID 1H97; Petitpas et al., 2001). The docking calculation of CS-866 to HSA was performed using SYBYL FlexX (Rarey et al., 1996). CS-866 docked at site I and site II. The residues within 5 Å from *S*-warfarin were defined as site I, and the residues within 5 Å from myristate-3 and -4 were defined as site II. During the docking calculation, the structure of HSA was kept rigid. The docking algorithm generated 275 and 209 different placements of CS-866 in site I and site II, respectively. All placements were evaluated using the scoring function of FlexX. For each site, because the top 10 placements exhibited nearly identical binding modes, we chose the placement with the best value as the candidate binding mode.

Refinement of Docking Models. To refine the docking models, the coordinates of CS-866 and the residues within 10 Å from CS-866 were optimized to reduce the root mean square of the gradients of potential energy to below 0.05 kcal mol^{-1} Å^{-1} using SYBYL 6.9.1 (Tripos, Inc., St. Louis, MO, 2003). The Tripos force field was used for the molecular energy calculation. The AMBER 7 charges (Cornell et al., 1995) were used as the atomic charges for HSA. The Gasteiger-Hückel charges (Purcel and Singer, 1967; Gasteiger and Marsili, 1980; Marsili and Gasteiger, 1980, 1981) were used as the charges for CS-866. The cut-off distance for the nonbonded interactions was 10 Å. The distance-dependent dielectric constant of $4r$ was used. Due to the lack of the 1st and 2nd N-terminal residues and the lack of the 585th C-terminal residue in the crystal structure of HSA, the 3rd and 584th residues were protected by an acetyl group and by an *N*-methyl group, respectively. The initial positions of the other missing atoms in the crystal structure were generated by SYBYL.

Statistics. Where possible, statistical analyses were performed using Student's *t* test

Results

Hydrolytic Kinetics. First, we were able to confirm that the hydrolysis of CS-866 by HSA followed Michaelis-Menten kinetics (data not shown). Table 1 shows the K_M, V_{max}, k_{cat}, and specificity constant (k_{cat}/K_M) values for the hydrolytic reaction.

To elucidate the reactivity of CS-866, we compared the kinetic parameters for CS-866 with those determined for the release of *p*-nitrophenol from PNPA (Table 2) (Means and Bender, 1975; Sakurai et al., 2004). The K_S value was found to be lower for CS-866,

TABLE 1

Kinetic parameters for the hydrolytic reaction between CS-866 and HSA at pH 7.4 and 37°C

HSA Type	K_M	V_{max}	k_{cat}	k_{cat}/K_M
	μM	$nmol \cdot min^{-1}$	min^{-1}	$\mu M^{-1} \cdot min^{-1}$
Native	48.2	1.02	0.113	0.00232

[a] Reaction conditions: 75 μM HSA, 10 to 250 μM CS-866, 1/15 M phosphate buffer (pH 7.4), 37°C.

TABLE 2

Kinetic parameters for the hydrolysis of CS-866 and PNPA by HSA at pH 7.4 and 25°C

Substrate	k_{cat}	K_S	k_{cat}/K_S
	$10^{-2} \cdot s^{-1}$	μM	$M^{-1} \cdot s^{-1}$
CS-866	0.845	42.5	19.9
PNPA	86.8	217	403.4

[a] PNPA data from Sakurai et al. (2004).

TABLE 3

Thermodynamic parameters for the hydrolysis of CS-866 and PNPA by HSA

Substrate	ΔG_1	ΔG_S	ΔG	ΔH	ΔS
	$kJ \cdot mol^{-1}$	$kJ \cdot mol^{-1}$	$kJ \cdot mol^{-1}$	$kJ \cdot mol^{-1}$	$kJ \cdot mol^{-1} \cdot K^{-1}$
CS-866	71.3	−25.0	96.3	34.7	−0.207
PNPA[a]	58.1	−20.9	79.0	66.1	−0.0435

[a] PNPA data from Sakurai et al. (2004). Reaction conditions: 1/15 M phosphate buffer (pH 7.4), 25°C.

suggesting that PNPA has greater affinity than CS-866 for HSA (Fersht, 1998; Sakurai et al., 2004). The catalytic rate constant, k_{cat}, was also found to be greater for PNPA.

Thermodynamics. The relationship between the catalytic rate constants and temperature followed the Arrhenius equation. Accordingly, a linear relationship was found between ln k_{cat} and $1/T$, where T is the absolute temperature in degrees Kelvin (data not shown). The activation energy of the reaction, E_a, calculated from the Arrhenius plot (Fersht, 1998; Sakurai et al., 2004), was found to be 37.1 kJ · mol^{-1}.

Using the HSA-hydrolysis parameters, we compared energy changes and thermodynamic parameters between CS-866 and PNPA (Table 3). CS-866 had larger values of ΔG (96.3 kJ · mol^{-1}) and ΔS (−0.207 kJ · mol^{-1} · K^{-1}) than PNPA.

Effects of Ligands on Hydrolysis. The site I-specific ligands warfarin, DNSA, and *n*-butyl *p*-AB were used as inhibitors to investigate for any competition with the hydrolytic reaction (Yamasaki et al., 1996; Kragh-Hansen et al., 2002). Interestingly, warfarin inhibited hydrolysis in a competitive manner, with a K_i value of 155 μM in a Dixon plot (Fig. 2A). By contrast, neither *n*-butyl *p*-AB nor DNSA inhibited HSA-catalyzed hydrolysis of CS-866 (Fig. 2, B and C).

The site II-specific ligands ibuprofen and diazepam were used to investigate, whether there is competition between that ligand-binding site and the catalytic site (Kragh-Hansen et al., 2002). Diazepam had no inhibitory effect, but competitive inhibition was observed with ibuprofen, with a K_i value of 235 μM in a Dixon plot (Fig. 3A and 3B).

Effect of Chemical Modification on Hydrolysis. Hydrolytic activities of the four specifically modified HSA derivatives (Tyr-, Lys-, His-, and Trp-HSA) were assayed (Fig. 4). Compared with native-type HSA, all modified HSA derivatives had significantly decreased hydrolytic activity ($p < 0.05$). Modification of Lys residues or of the single Trp residue resulted in the most pronounced reductions in catalytic reactivity.

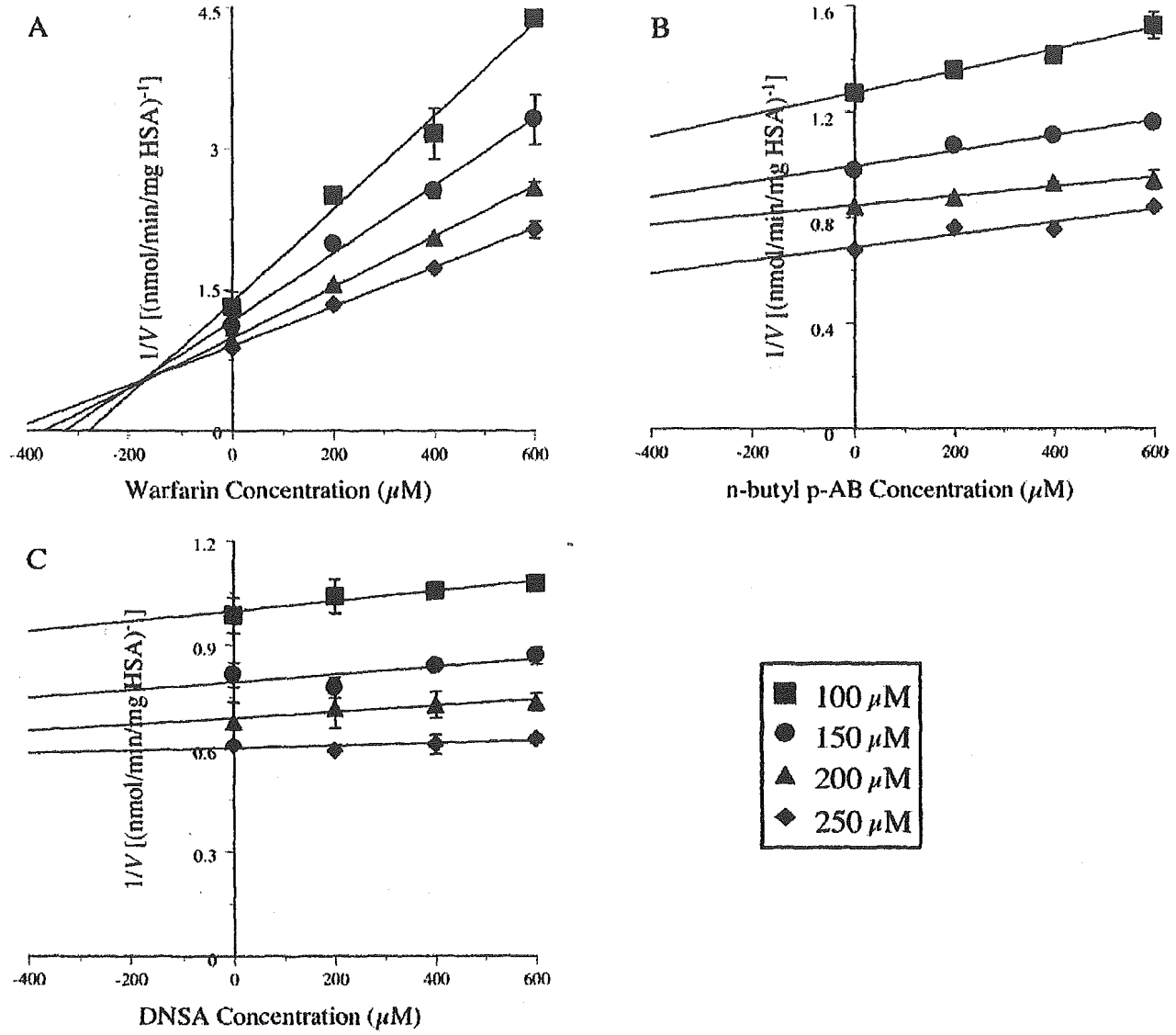

FIG. 2. Effect of warfarin (A), *n*-butyl *p*-AB (B), and DNSA (C) (0–600 μM) on the hydrolysis of CS-866 by HSA. Reaction conditions: 75 μM HSA, 100 to 250 μM CS-866, 1/15 M phosphate buffer (pH 7.4), 37°C. Plots represent mean ± S.D. ($n = 3$).

Examination of Hydrolytic Activity Using Site-Directed Mutagenesis. Wild-type rHSA and the HSA single-residue mutants K199A, W214A, and Y411A were used to examine involvement of various amino acid residues in the hydrolysis. The hydrolytic activity of each rHSA was examined to elucidate the contribution of specific amino acid residues (Fig. 5). Compared with the wild-type rHSA, all mutant rHSAs showed significant decreases in catalytic activity. K199A exhibited a particularly marked decrease in catalytic activity ($p < 0.01$), suggesting that Lys-199 plays a particularly important role in the hydrolysis. These results are in good agreement with those obtained with the chemically modified HSAs. The W214A and Y411A mutants showed a significant reduction in catalytic activity ($p < 0.05$), indicating that the amino acid residues Trp-214 and Tyr-411 are also involved in the hydrolytic reaction.

Molecular Interaction of CS-866 and HSA in Docking Models. We obtained two docking models: model I for site I, and model II for site II. In model I, the binding of CS-866 was similar to that of warfarin (Fig. 6). The biphenyl moiety of CS-866 was bound to the hydrophobic pocket consisting of Leu-219, Leu-238, Val-241, Leu-260, Ala-261, Ile-264, Ile-290, and Ala-291. The 2-propyl-imidazole moiety and the propan-2-ol moiety were bound to the other hydrophobic pocket (Phe-211, Trp-214, Ala-215, Leu-219, and Leu-238). Hydrogen bonds to and electrostatic interactions with other residues are detailed in Table 4. Oxygen atoms of the vinylene carbonate moiety formed hydrogen bonds with side chains of Arg-218 and of Arg-222. Negative charges of the tetrazole moiety interacted electrostatically with side chains of Lys-199 and of Arg-257. The hydroxyl oxygen atom of the propan-2-ol moiety formed a hydrogen bond with the side chain of Lys-199, and the hydrogen atom formed a hydrogen bond with the side chain of His-242. The carbonyl oxygen atom of the ester moiety formed a hydrogen bond with the side chain of Lys-199. The ester moiety of CS-866 was in the vicinity of Glu-292. However, the side chain of Glu-292 was distant from the carbonyl carbon of the ester moiety, because the docking program, FlexX, cannot account for chemical reactions and remains rigid. We changed the torsion angles

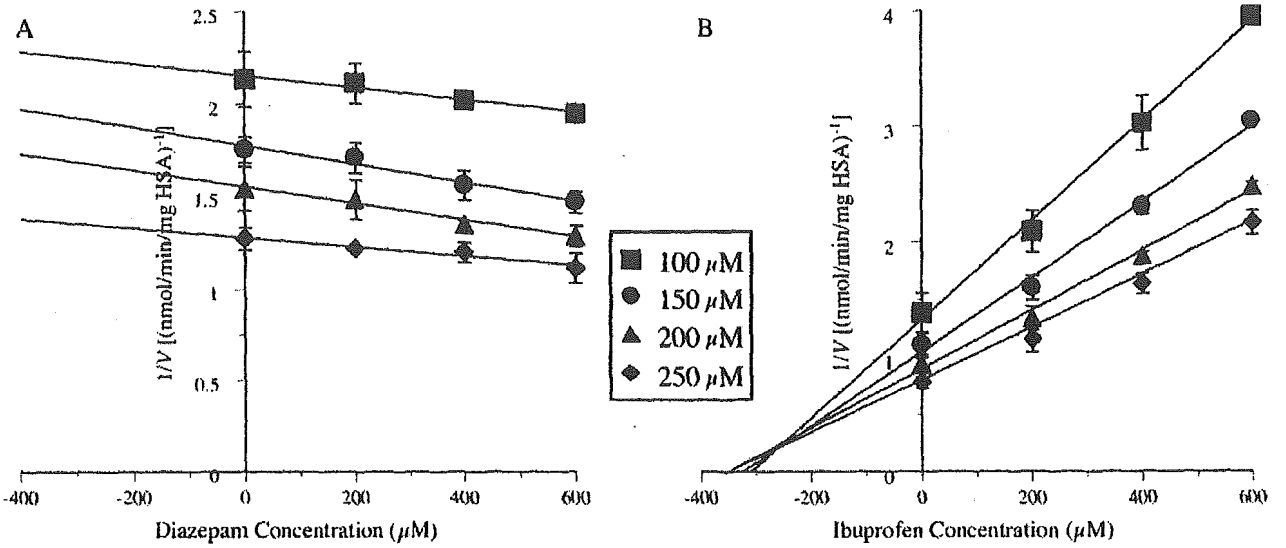

FIG. 3. Effect of diazepam (A) and ibuprofen (B) (0–600 μM) on the hydrolysis of CS-866 by HSA. Reaction conditions: 75 μM HSA, 100 to 250 μM CS-866, 1/15 M phosphate buffer (pH 7.4), 37°C. Plots represent mean ± S.D. (n = 3).

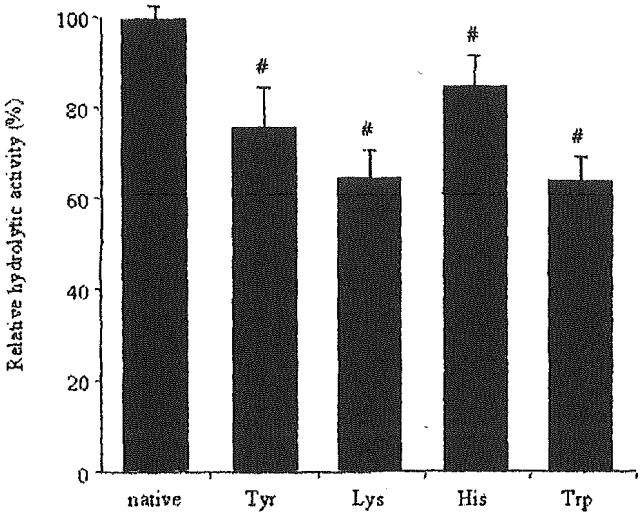

FIG. 4. Hydrolytic activities of chemically modified HSAs as compared with that of normal HSA. Reaction conditions: 75 μM HSA, 250 μM CS-866, 1/15 M phosphate buffer (pH 7.4), 37°C. Each column represents mean ± S.D. (n = 3). #, significantly different from native-type HSA ($p < 0.05$).

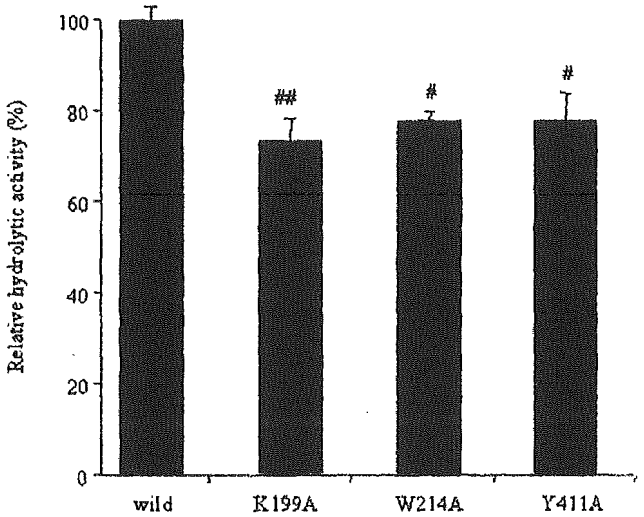

FIG. 5. Hydrolytic activities of mutant rHSAs as compared with that of wild-type rHSA. Reaction conditions: 75 μM HSA, 250 μM CS-866, 1/15 M phosphate buffer (pH 7.4), 37°C. Each column represents mean ± S.D. (n = 3). #, $p < 0.05$, and ##, $p < 0.01$ as compared with wild-type rHSA.

of the side chain of Glu-292 without steric hindrance as Glu-292 became capable of a nucleophilic reaction.

In model II, CS-866 was bound to site II using the pocket for myristate-4 (Fig. 7) (Curry et al., 1998). The pocket for myristate-3 was not occupied. The biphenyl moiety and the 2-propyl-imidazole moiety were bound to the hydrophobic pocket consisting of Leu-387, Pro-486 and Ala-490. The propan-2-ol moiety was surrounded by the hydrophobic residues (Leu-387, Leu-430, and Leu-453). Table 5 shows hydrogen bonds and electrostatic interactions in site II. Negative charges of the tetrazole moiety interacted electrostatically with the side chain of Arg-485, and the tetrazole moiety formed a hydrogen bond with the side chain of Asn-391. The side chain of Ser-489 formed hydrogen bonds with the hydroxyl oxygen atom of the propan-2-ol moiety and the carboxyl oxygen atom of the ester moiety. The carbonyl oxygen atom of the ester moiety formed a hydrogen bond with the side chain of Lys-414. The carboxyl oxygen atom of the ester moiety formed a hydrogen bond with the side chain of Tyr-411.

Discussion

This antihypertensive prodrug, CS-866, is hydrolyzed in the serum. Hydrolysis of CS-866 in serum has been observed in several species, and comparison among five species has shown that hydrolytic activity is highest in rabbits, followed by dogs, mice, rats, and humans (Ikeda, 2000). Furthermore, we examined the activity due to serum albumin. It was found to be highest in humans, followed by rats, mice, rabbits, and dogs (data not shown). This indicates that the mechanisms of hydrolysis of CS-866 in serum differ among those species, and that HSA plays a more important role in producing RNH-6270 than other serum albumin species.

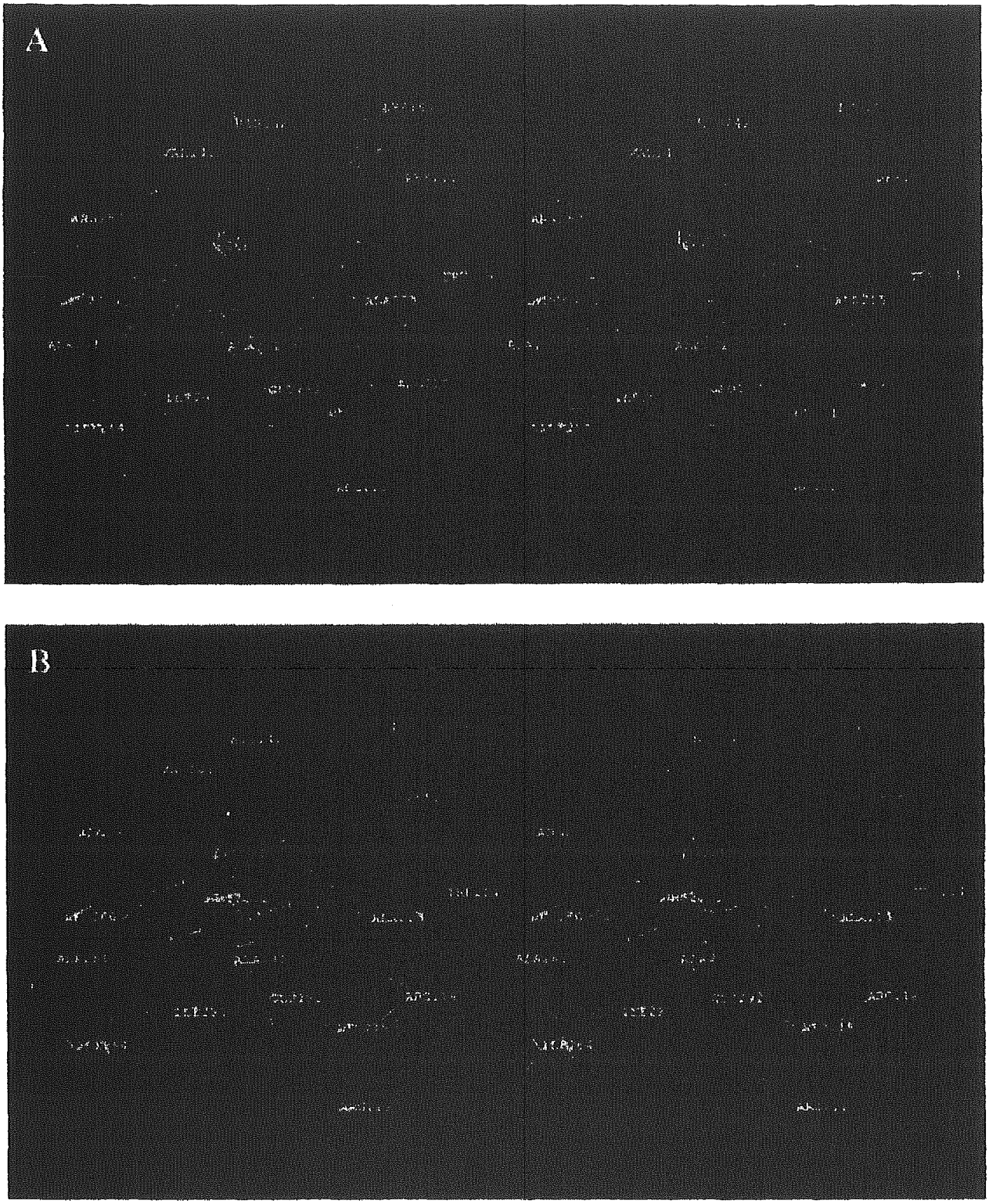

FIG. 6. Stereo drawings of ligands in site I. A, modeling structure for CS-866. The torsion angles of the side chain of Glu-292 were changed as Glu-292 becomes capable of a nucleophilic reaction. B, crystal structure for *S*-warfarin (PDB ID 1H9Z). Relaxed stereo viewing.

TABLE 4

Hydrogen bonds and electrostatic interactions in model I of HSA-CS-866 complex

Donor		Acceptor		Distance
				Å
Hydrogen bonds				
Lys-199	N_ζ	Ester	C=O	4.1
	N_ζ	Propan-2-ol	OH	3.0
Propan-2-ol	OH	His-242	Nε2	4.6
Arg-218	N_ε	Vinylene carbonate	O2	3.8
	$N_\eta 2$		C=O	3.4
Arg-222	$N_\eta 2$		C1	3.1
Positive		Negative		
Electrostatic interactions				
Lys-199	N_ζ	Tetrazole	N2	5.7
Arg-257	N_ε		N4	2.8

Thermodynamic Properties. The esterase-like activity of HSA is dependent on the catalytic rate constant, k_{cat}, and increases with a decrease in the activation free energy change, ΔG. Thus, the magnitude of ΔG, which is dependent on activation entropy change (ΔS), as calculated from a thermodynamic analysis, can be regarded as an indicator of hydrolytic activity of HSA (Fersht, 1998; Sakurai et al., 2004). Because PNPA has lower ΔG and ΔS values than CS-866 (Table 3), PNPA exhibited greater affinity for HSA and a higher catalytic rate than CS-866 (Table 2). Hydrolysis reactions catalyzed by albumin have previously been found to have a particularly great entropy difference between the ground state (ES) and the transition state (ES*) (Sakurai et al., 2004). The active sites of HSA to which the substrate binds are perfectly oriented to the reactive site of the substrate (the ester portion) for hydrolysis, and thus has a smaller entropy difference between the transition state (ES*) and the ground state (ES). This may be the reason why hydrolysis of PNPA proceeds more readily than hydrolysis of CS-866. That is, compared to CS-866, PNPA has a structure and orientation that are better suited to hydrolysis by HSA.

Relationship Between Ligand Binding Sites and Hydrolytic Active Sites. HSA is the most abundant protein in blood plasma and serves as a storage protein and transport protein for many endogenous and exogenous compounds (Peters, 1996; Kragh-Hansen et al., 2002). The unique capability of HSA to reversibly bind a large number of compounds is usually explained by the existence of a number of binding regions (including site I and site II), each of which has a very different specificity (Kragh-Hansen, 1991; Kragh-Hansen et al., 2002). Furthermore, site I on HSA consists of three subsites: Ia, Ib, and Ic (Fehske et al., 1982; Yamasaki et al., 1996). Another important role of HSA is as a catalyst for the hydrolysis of various compounds, such as esters, amides, and phosphates. It has been suggested that the active site of HSA for *p*-nitrophenyl esters is site II, and that Tyr-411 is essential for hydrolysis of *p*-nitrophenyl esters (Ozeki et al., 1980; Watanabe et al., 2000). The reactive site and active residue for nitroaspirin are reportedly site I and Lys-199, respectively (Ikeda and Kurono, 1986). The relationship between the hydrolytic active sites of HSA for CS-866 and the proteins' ligand-binding sites was investigated in the present study.

There are interesting patterns of competition between site I and site II ligands for hydrolysis. Although warfarin, which is regarded as a typical ligand of subsite Ia of HSA, acts as a competitive inhibitor, this does not necessarily indicate that the HSA catalytic site for CS-866 is subsite Ia, because ibuprofen, a typical site II ligand, also exhibited evidence of competitive inhibition (Figs. 2A and 3B). These results suggest that substrate specificity of the esterase-like region and ligand-binding site of HSA is inconsistent. In other words, the catalytic site for CS-866 on HSA may recognize CS-866 in a manner different from that of the ligand-binding site.

Roles of Specific Amino Acid Residues. For proteins whose X-ray crystallographic structure is known, the role of each amino acid residue can be quantitatively determined using the amino acid displacement (site-directed mutagenesis) technique and information obtained from X-ray analysis.

The present chemical modification experiments indicate that Lys, Trp, and Tyr residues of HSA are important for hydrolysis of CS-866 by HSA, and that His residues are also involved (Fig. 4). These experiments were performed with mildly modified HSA, because, for example, only 1.2% of the Tyr residues and 3.8% of the Lys residues were modified. However, HSA has 59 Lys residues, and the numbers of Trp, Tyr, and His residues are 1, 18, and 16, respectively. Previous findings have demonstrated that Tyr-411 is most likely the reactive Tyr of HSA (Watanabe et al., 2000). It is also known that the reactivity of Lys-199 is high (Means and Bender, 1975). Furthermore, it is reported that this single Trp residue contributes to the esterase-like activity of HSA (Ozeki et al., 1980; Kurono et al., 1982). In an attempt to identify specific residues of importance for the hydrolysis of CS-866, we examined the activity of several rHSAs, namely wild-type HSA and the single-residue mutants K199A, W214A, and Y411A.

Because we did not observe a great decrease of the hydrolytic activity of HSA for CS-866, even in the single-residue mutants K199A and Y411A, we conclude that the catalytic sites of HSA for CS-866 are not solely confined to the Lys-199 and Tyr-411 residues but, rather, involves several additional amino acid residues (Fig. 5).

The single Trp residue, Trp-214, is located close to Lys-199, as indicated by X-ray diffraction analysis, and is an element of a major interdomain cluster of hydrophobic residues (He and Carter, 1992; Sugio et al., 1999). The mutant W214A exhibited a significant decrease in hydrolytic activity (Fig. 5). In addition, the microenvironment near Trp-214 was investigated to obtain detailed information about the role of this residue in the hydrolysis. After incubation with CS-866 for 10 min, the relative fluorescence intensity of HSA decreased by more than half and the λ_{max} was blue-shifted (data not shown). These results are consistent with a model indicating that the Trp-214 residue is involved in hydrolytic reaction. These limited data lead us to the idea that a double (or triple) mutation of Lys-199, Trp-214, and Tyr-411 could completely abolish the hydrolytic activity. Further investigations on this point are under way at this laboratory.

Structural Mechanism of Hydrolysis Based on Models. The present findings suggest that HSA has two catalytic sites for CS-866, for the following two reasons. Mutation at site I or site II diminishes but does not abolish the hydrolytic activity. The hydrolytic activity is inhibited by both warfarin (site I drug) and ibuprofen (site II drug).

In model I (Fig. 6), CS-866 occupied the binding site of warfarin; this is consistent with the results showing that warfarin inhibits the hydrolytic activity of HSA. In site I, the carbonyl oxygen atom of the ester moiety formed a hydrogen bond with the side chain of Lys-199, and this hydrogen bond could function as an oxyanion hole. The importance of Lys-199 indicated by the model is consistent with the decreased hydrolytic activity of the K199A mutant and the HSA variant produced by chemical modification of Lys. The catalytic residue may be Glu-292; the distance between the oxygen atom of the side chain of Glu-292 and the carbonyl carbon of the ester moiety of CS-866 was 4.8 Å. The hydrophobic interaction between CS-866 and Trp-214 indicated by the model is consistent with the diminished

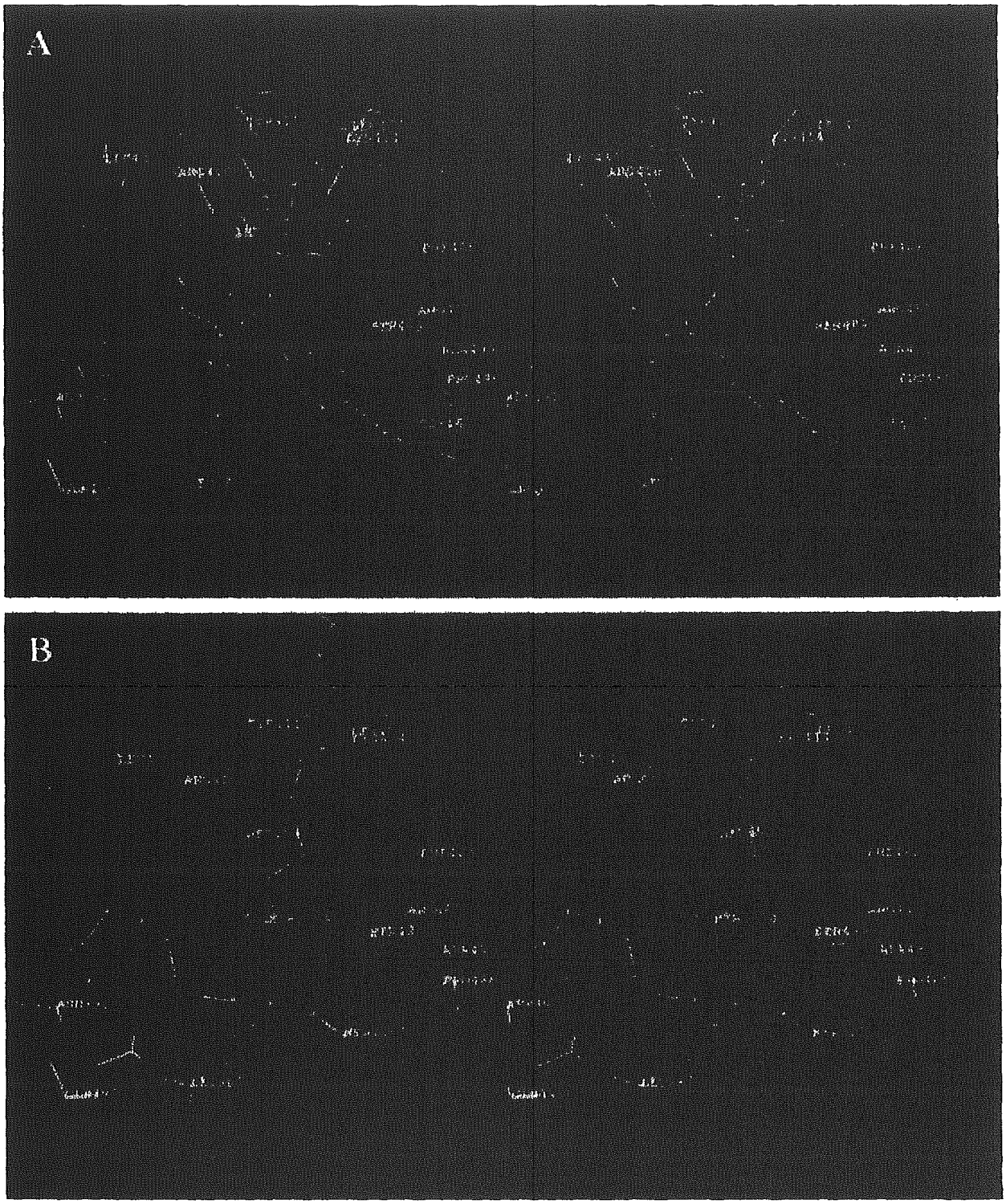

FIG. 7. Stereo drawings of ligands in site II. A, modeling structure for CS-866; B, crystal structure for myristate-3 and -4 (PDB ID 1H9Z). Relaxed stereo viewing.

hydrolytic activity of the W214A mutant and the HSA variant produced by chemical modification of Trp.

Model II (Fig. 7) indicates that the mechanism of hydrolysis of CS-866 is almost the same as that found in previous studies for *p*-nitrophenyl esters, with the exception of the involvement of Arg-410 (Watanabe et al., 2000; Sakurai et al., 2004). Instead of Arg-410, Lys-414 was used to create an oxyanion hole. The distance between the hydroxyl oxygen atom of Tyr-411 and the carbonyl carbon of the

TABLE 5

Hydrogen bonds and electrostatic interactions in model II of HSA-CS-866 complex

Donor		Acceptor		Distance
				Å
Hydrogen bonds				
Asn-391	$N_{\delta}2$	Tetrazole	N2	2.9
Tyr-411	O_{η}	Ester	–O–	2.8
Lys-414	N_{η}		C=O	2.7
Ser-489	O_{γ}		–O–	4.7
	O_{γ}	Propan-2-ol	OH	4.1
Positive		Negative		
Electrostatic interactions				
Arg-485	$N_{\eta}1$	Tetrazole	N3	3.5

ester moiety of CS-866 was 3.3 Å, indicating that it is possible that Tyr-411 plays the role of a catbartic residue. The importance of Tyr-411 and Lys-414 is consistent with the decreased hydrolytic activity of the Y411A mutant and of the HSA variants produced by chemical modification of Tyr or Lys. In our model II, CS-866 was bound to the pocket for myristate-4 in site II. The binding pockets of the site II ligands ibuprofen and diazepam are unknown. If ibuprofen binds to the pocket for myristate-4, our model II provides a mechanism for inhibition of hydrolytic activity of HSA by ibuprofen.

The present findings indicate that hydrolysis of CS-866 by HSA is dependent on ΔS. Another important factor is the orientation between the catalytic active site on HSA and the ester region of the substrate. There are differences between the catalytic active sites and the ligand-binding sites of HSA. Furthermore, the residues of Lys-199, Trp-214, and Tyr-411 play important roles in this catalytic reaction. All of these experimental findings are consistent with the docking model that we derived from computer simulation.

References

Brousil JA and Burke JM (2003) Olmesartan medoxomil: an angiotensin II-receptor blocker. *Clin Ther* **25**:1041–1055.

Chen RF (1967) Removal of fatty acids from serum albumin by charcoal treatment. *J Biol Chem* **242**:173–181.

Curry S, Mandelkow H, Brick P, and Franks N (1998) Crystal structure of human serum albumin complexed with fatty acid reveals an asymmetric distribution of binding sites. *Nat Struct Biol* **5**:827–835.

Cornell WD, Cieplak P, Bayly CI, Gould IR, Merz KM Jr, Ferguson DM, Spellmeyer DC, Fox T, Caldwell JW, and Kollman PA (1995) A second generation force field for the simulation of proteins, nucleic acids and organic molecules. *J Am Chem Soc* **117**:5179–5197.

Fehske KJ, Müller WE, and Wollert U (1978) The modification of the lone tryptophan residue in human serum albumin by 2-hydroxy-5-nitrobenzyl bromide. Characterization of the modified protein and the binding of L-tryptophan and benzodiazepines to the tryptophan-modified albumin. *Hoppe-Seylers Z Physiol Chem* **359**:709–717.

Fehske KJ, Schläter U, Wollert U, and Müller WE (1982) Characterization of an important drug binding area on human serum albumin including the high-affinity binding sites of warfarin and azapropazone. *Mol Pharmacol* **21**:387–393.

Fersht A (1998) *Structure and Mechanism in Protein Science*. Freeman, New York.

Gasteiger J and Marsili M (1980) Iterative partial equalization of orbital electronegativity: a rapid access to atomic charges. *Tetrahedron* **36**:3219–3228.

Gasteiger J and Marsili M (1981) Prediction of proton magnetic resonance shifts: the dependence on hydrogen charges obtained by iterative partial equalization of orbital electronegativity. *Organ Magn Reson* **15**:353–360.

Gounaris AD and Perlmann GE (1967) Succinylation of pepsinogen. *J Biol Chem* **242**:2739–2745.

Haynes R, Osuga DT, and Feeney RE (1967) Modification of amino groups in inhibitors of proteolytic enzymes. *Biochemistry* **6**:541–547.

He XM and Carter DC (1992) Atomic structure and chemistry of human serum albumin. *Nature (Lond)* **358**:209–215.

Ikeda K and Kurono Y (1986) Enzymatic activity and drug binding activity of human serum albumin. *Yakugaku Zasshi* **106**:841–855.

Ikeda T (2000) Two prodrugs activated by serum esterases including albumin. Proceedings of the International Symposium on Serum Albumin & α_1-Acid Glycoprotein 173–180.

Koike H, Sada T, and Mizuno M (2001) In vitro and in vivo pharmacology of olmesartan medoxomil, an angiotensin II type AT1 receptor antagonist. *J Hypertens Suppl* **19**: 1:S3–S14.

Kragh-Hansen U (1991) Octanoate binding to the indole- and benzodiazepine-binding region of human serum albumin. *Biochem J* **273**:641–644.

Kragh-Hansen U, Chuang VTG, and Otagiri M (2002) Practical aspects of the ligand-binding and enzymatic properties of human serum albumin. *Biol Pharm Bull* **25**:695–704.

Kurono Y, Yamada H, and Ikeda K (1982) Effects of drug binding on the esterase-like activity of human serum albumin. V. Reactive site towards substituted aspirins. *Chem Pharm Bull* **30**:296–301.

Marsili M and Gasteiger J (1980) Pi-Charge Distributions from Molecular Topology and Pi-Orbital Electronegativity. *Croat Chem Acta* **53**:601–614.

Means GE and Bender ML (1975) Acetylation of human serum albumin by p-nitrophenyl acetate. *Biochemistry* **14**:4989–4994.

Neutel JM (2001) Clinical Studies of CS-866, the newest angiotensin II receptor antagonist. *Am J Cardiol* **87** (8A):37C–43C.

Ozeki Y, Kurono Y, Yotsuyanagi T, and Ikeda K (1980) Effects of drug binding on the esterase activity of human serum albumin: inhibition modes and binding sites of anionic drugs. *Chem Pharm Bull* **28**:535–540.

Peters T Jr (1996) *All about Albumin, Biochemistry, Genetics and Medical Applications*. Academic Press, San Diego.

Petitpas I, Bhattacharya AA, Twine S, East M, and Curry S (2001) Crystal structure analysis warfarin binding to human serum albumin: anatomy of drug site I. *J Biol Chem* **276**:22804–22809.

Purcel WP and Singer JA (1967) A brief review and table of semiempirical parameters used in the Hückel molecular orbital method. *J Chem Eng Data* **12**:235–246.

Rarey M, Kramer B, Lengauer T, and Klebe G (1996) A fast flexible docking method using incremental construction algorithm. *J Mol Biol* **261**:470–489.

Roosemont JL (1978) Reaction of histidine residues in proteins with diethylpyrocarbonate: differential molar absorptivities and reactivities. *Anal Biochem* **88**:314–320.

Sakurai Y, Ma SF, Watanabe H, Yamaotsu N, Hirono S, Kurono Y, Kragh-Hansen U, and Otagiri M (2004) Esterase-like activity of serum albumin: characterization of its structural chemistry using p-nitrophenyl esters as substrates. *Pharm Res (NY)* **21**:285–292.

Sokolovsky M, Riordan JF, and Vallee BL (1966) Tetranitromethane. A reagent for the nitration of tyrosyl residues in proteins. *Biochemistry* **5**:3582–3589.

Sugio S, Kashima A, Mochizuki S, Noda M, and Kobayashi K (1999) Crystal structure of human serum albumin at 2.5 A resolution. *Protein Eng* **12**:439–446.

Watanabe H, Tanase S, Nakajou K, Maruyama T, Kragh-Hansen U, and Otagiri M (2000) Role of Arg-410 and Tyr-411 in human serum albumin for ligand binding and esterase-like activity. *Biochem J* **349**:813–819.

Watanabe H, Yamasaki K, Kragh-Hansen U, Tanase S, Harada K, Suenaga A, and Otagiri M (2001) In vitro and in vivo properties of recombinant human serum albumin from Pichia pastoris purified by a method of short processing time. *Pharm Res (NY)* **18**:1775–1781.

Yamasaki K, Maruyama T, Kragh-Hansen U, and Otagiri M (1996) Characterization of site I on human serum albumin: concept about the structure of a drug binding site. *Biochim Biophys Acta* **1295**:147–157.

Address correspondence to: Professor Masaki Otagiri, Ph D., Department of Biopharmaceutics, Graduate School of Pharmaceutical Sciences, Kumamoto University, 5-1 Oe-honmachi, Kumamoto 862-0973, Japan. E-mail: otaginm@gpo.kumamoto-u.ac.jp

Stereostructure of luminamicin, an anaerobic antibiotic, via molecular dynamics, NMR spectroscopy, and the modified Mosher method

Hiroaki Gouda*, Toshiaki Sunazuka†, Hideaki Ui*, Masaki Handa*, Yusuke Sakoh*, Yuzuru Iwai†, Shuichi Hirono*‡, and Satoshi Ōmura†‡

*School of Pharmaceutical Sciences, Kitasato University, Shirokane, Minato-ku, Tokyo 108-8641, Japan; and †Kitasato Institute for Life Sciences, Graduate School of Infection Control Sciences, Kitasato University, and The Kitasato Institute, Shirokane, Minato-ku, Tokyo 108-8641, Japan

Contributed by Satoshi Ōmura, September 28, 2005

The absolute stereostructure of luminamicin, an anaerobic antibiotic, has been determined by using conformational analysis via high-temperature molecular dynamics, NMR spectroscopy, and the modified Mosher method. It was found that luminamicin has the *S*, *S*, *R*, *R*, *R*, *S*, *S*, *S*, *R*, and *S* configurations at C2, C4, C7, C9, C10, C11, C12, C13, C16, C28, and C29, respectively. This configuration is the same as that found in nodusmicin, which has a chemical structure quite similar to luminamicin. The structure of luminamicin consists of three different rings, i.e., a decalin ring, a 10-membered macrolactone ring, and a 14-membered macrolactone ring. The resulting three-dimensional structure of luminamicin shows an interesting feature in that the maleic anhydride functionality in conjugation with the enol ether group of the 14-membered macrolactone is nearly perpendicular to the plane of the other two rings.

The emergence of resistance against generally used antibiotics will be a long-lasting serious clinical problem. We need to continue developing new medicines that have unique mechanisms of action. We have found previously uncharacterized antianaerobe antibiotics of actinomycetes origin, thiotetromycin (1), clostomicin (2), luminamicin (3), and lustromycin (4, 5). The structure of luminamicin (Fig. 1) was identical to that of coloradocin, which was isolated by McAlpine (6). Luminamicin showed selective activity against anaerobic and microaerophilic bacteria, including pathogenic species of *Clostridium*, *Neisseria*, and *Haemophilus*, whereas it was not active against most aerobic bacteria (3, 6). Interestingly, structurally related antibiotics, nodusmicin (7) and nargenicin (8), are reported to inhibit some aerobic bacteria. Therefore, the additive macrocyclic structure of luminamicin seems to be important in exerting its selective antianaerobic microbial activity. In conjunction with our continuing program directed toward the structure elucidation and synthesis of important antimicrobial natural products, we describe here the elucidation of the absolute stereochemistry of luminamicin.

The preliminary NMR study of luminamicin could explain only relative configuration with respect to C4, C7, C9, C10, C11, C12, and C13, but could not provide any absolute configuration of chiral carbon atoms of luminamicin (6). Recently, we have determined the stereostructure of choloropeptin I, an unusual chlorinated hexapeptide with selective anti-HIV activities, by inhibiting the binding between HIV gp120 envelope protein and CD4 protein, using a combination method of conformational analysis via high-temperature molecular dynamics (MD) and NMR spectroscopy (9–11). Among six amino acids involved in choloropeptin I, three were established to be all *R* configurations by acidic hydrolysis, but the other three had not been assigned. In that study, we just needed to consider eight different diastereomers. Therefore, NMR spectroscopy has been applied successfully to determine the stereochemistry of choloropeptin I. However, in the case of luminamicin, we have no absolute configuration of chiral carbon atoms and need to consider both diastereomers and enantiomers. Therefore, only applying NMR spectroscopy is not enough to determine the *absolute* stereochemistry of luminamicin, because it can provide only *relative* structural information. However, the modified Mosher method is well known to give an absolute configuration for a chiral carbon atom with a hydroxyl group (12, 13). Luminamicin has two chiral carbon atoms attached to a hydroxyl group. Therefore, we can expect that the modified Mosher method will be able to assign an absolute configuration for each of these carbons atoms. In this study, we use a combination of conformational analysis via high-temperature MD, NMR spectroscopy, and the modified Mosher method to determine the absolute stereochemistry of luminamicin. Once we obtain at least one absolute configuration by the modified Mosher method, we can assign absolute configurations for other chiral carbon atoms using relative structural information derived from NMR spectroscopy. We will show that this combination method is very powerful, even when it is necessary to consider both diastereomers and enantiomers.

Methods

NMR Experiments. Luminamicin (1) was prepared as described in ref. 3. The sample of 10 mg was dissolved in 0.6 ml of $CDCl_3$. All NMR spectra were recorded on a Varian INOVA600 spectrometer operating at 600 MHz for the proton frequency at 30°C. A relaxation delay of 2.0 s was used in all experiments. The 1D proton spectrum used to estimate coupling constants was measured with a spectral width of 9,012 Hz and a data block size of 27,000, so the digital resolution was 0.67 Hz per point. An unshifted sine bell was applied to the free induction decay NMR signal. Chemical shifts were referenced with respect to residual solvent signal (7.26 ppm).

For calculation of distance constraints, the rotating-frame Overhauser effect (ROE) data were collected by the 2D-TROESY (transverse rotating-frame Overhauser effect spectroscopy) pulse sequence of Hwang and Shaka (14, 15) with mixing times of 100, 150, 200, 250, and 300 ms, which is designed to suppress total correlation spectroscopy cross peaks. The spinlock pulse was $180°(x)\ 180°(-x)$, with a field strength of 6,200 Hz. 2D-TROESY spectroscopy was performed with a spectral width of 5,273 Hz in the phase-sensitive mode (16). A total of 512 blocks were acquired with data points of 2,048. Before 2D Fourier transformation, the acquired data were multiplied by a Gauss function in t2 and by a shifted sine square function in t1 and were zero-filled once along the t1 direction.

Conflict of interest statement: No conflicts declared.

Abbreviations: MD, molecular dynamics; ROE, rotating-frame Overhauser effect; TROESY, transverse rotating-frame Overhauser effect spectroscopy.

‡To whom correspondence may be addressed. E-mail: hironos@pharm.kitasato-u.ac.jp or omura-s@kitasato.or.jp.

www.pnas.org/cgi/doi/10.1073/pnas.0508425102

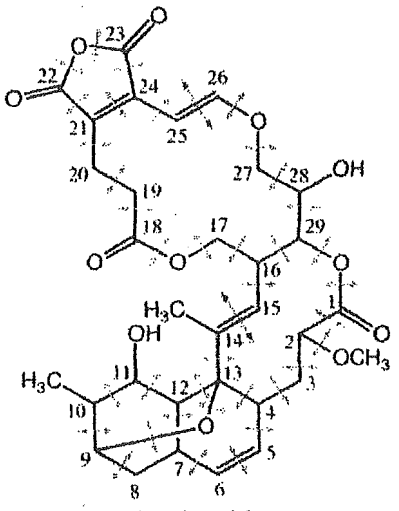

Fig. 1. Chemical structure of luminamicin. The dihedral angles used to cluster similar conformers are indicated by blue arrows. The dihedral angles constrained to be tarns in MD calculations are indicated by red dashed arrows.

Conformational Analysis of Luminamicin. The preliminary NMR study of luminamicin (1) suggested that there are only two possible absolute configurations on a decalin ring system including C4–C13, i.e., the *R*, *S*, *S*, *S*, *S*, *R*, and *R* or the *S*, *R*, *R*, *R*, *R*, *S*, and *S* configurations at C4, C7, C9, C10, C11, C12, and C13, respectively (Fig. 2). Therefore, we first prepared initial structures of the 16 diastereomers differing in the configuration at C2, C16, C28, and C29 for luminamicin with either of these two decalin configurations, using SYBYL 6.91 (Tripos, St. Louis). As a result, a total of 32 initial structures were prepared. Then, the conformational analysis of these initial structures was performed by using the program CAMDAS 2.1 (Conformational Analyzer with Molecular Dynamics and Sampling) (17). This program, developed in our laboratory, generates the energetically stable conformations of a target molecule by performing the high-temperature MD calculation and sampling conformations along the MD trajectory. CAMDAS then clusters similar conformations based on values of dihedral angles defined before calculation. The following calculations were performed for each initial structure by using CAMDAS. Ten MD calculations were simultaneously performed by using different conformers. Each of the MD calculations was carried out for 1,000 ps with an integral time step of 1 fs. The lengths of covalent bonds were fixed with SHAKE algorithm through the MD (18). The temperature of the system was maintained at 1,200 K to enhance the sampling efficiency. The Merck Molecular Force Field was used to evaluate the potential energy surface of the molecule (19). To mimic the shield effects of solvent molecules on electrostatic interactions, the electrostatic potential term was neglected. The 14-methyl group was suggested to be trans to H15 by its ^{13}C chemical shift value of 15.1 ppm (20). The H25 was also indicated to be trans to H26 on the basis of the large coupling constant between these protons of 13.5 Hz. Therefore, values of the dihedral angles of C13-C14-C15-C16 and H25-C25-C26-H26 were constrained to be 180° ± 10° in MD calculations to keep their conformations trans. The constraint energy term was quadratic, and the force constants were 100 kcal·mol^{-1}·rad^{-2}. Conformers were sampled at 100-step intervals, thus producing 10,000 conformations for each MD calculation. A total of 100,000 conformations were preclustered with a dihedral angles deviation threshold of ±30°. A total of 37 dihedral angles were

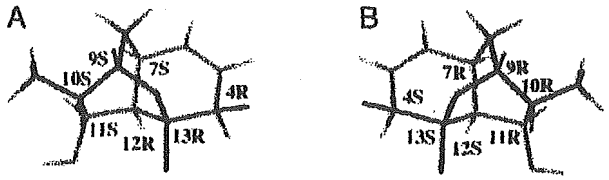

Fig. 2. Two possible stereostructures of the decalin ring of luminamicin. (*A*) C4, C7, C9, C10, C11, C12, and C13 have the *R*, *S*, *S*, *S*, *S*, *R*, and *R* configurations, respectively. (*B*) C4, C7, C9, C10, C11, C12, and C13 have the *S*, *R*, *R*, *R*, *R*, *S*, and *S* configurations, respectively.

used to cluster similar conformations, which are indicated by arrows in Fig. 1. Each of the conformers obtained after preclustering was then minimized until the root mean square (RMS) of the potential-energy gradient fell below 0.001 kcal·mol^{-1}·Å^{-1}. The minimized conformers were reclustered with a dihedral angle deviation threshold of ±30°, furnishing a final conformer set. All finally obtained conformers maintained chirality of their initial structures, although chirality restraints were not used in MD calculations. This result indicated that no inversion of chiral centers occurred during MD calculations.

Modified Mosher Method. ***28-[(+)-α-Methoxy-α-(trifluoromethyl)phenylacetoxy]luminamicin (2).*** To a solution of 1 (9.9 mg, 16.1 μmol) in CH_2Cl_2 (800 μl) at room temperature was added (+)-MTPA (11.3 mg, 48.3 μmol), EDCI [1-ethyl-3-(3-dimethylaminopropyl)carbodiimide] (9.3 mg, 48.3 μmol), and DMAP (4-dimethylaminopyridine) (0.4 mg, 3.22 μmol), and the mixture was stirred for 1 h and quenched with H_2O (5 ml). The resultant mixture was extracted with $CHCl_3$ (3 × 5 ml), and the combined extracts were washed with brine (5 ml), dried over Na_2SO_4, filtered, and concentrated. Flash column chromatography (Benzene/Acetone 20/1) furnished 2 (6.2 mg, 7.47 μmol, 46% yield) as a colorless solid: $[\alpha]_D^{25}$ +34.4 °(c 0.29, $CHCl_3$); TLC R_f 0.61 (Benzene/Acetone 2/1); mp 108–109°C; IR (KBr) 3,442, 1,761, 1,178 cm^{-1}; ^{1}H-NMR (600 MHz, $CDCl_3$) δ 0.98 (3H, d, *J* = 6.9 Hz), 1.42 (1H, m), 1.45 (1H, m), 1.69 (3H, s), 1.70 (1H, m), 1.80 (1H, m), 1.90 (1H, m), 2.19 (1H, m), 2.21 (1H, m), 2.48 (1H, m), 2.62 (1H, m), 2.72 (1H, m), 2.90 (1H, m), 2.96 (1H, m), 3.27 (3H, s), 3.34 (1H, m), 3.36 (1H, m), 3.64 (1H, m), 3.78 (1H, dd, *J* = 12.1, 5.0 Hz), 4.22 (1H, m), 4.26 (2H, m), 4.59 (1H, d, *J* = 12.1 Hz), 5.47 (1H, dd, *J* = 9.9, 2.5 Hz), 5.62 (1H, dd, *J* = 9.6, 5.5 Hz), 5.78 (1H, d, *J* = 13.5 Hz), 5.89 (1H, m), 5.90 (1H, d, *J* = 6.3 Hz), 6.04 (1H, dd, *J* = 9.6, 7.4 Hz), 7.91 (1H, d, *J* = 13.5 Hz); ^{13}C-NMR (150 MHz, $CDCl_3$) δ 15.1, 15.9, 18.7, 27.9, 29.6, 32.9, 33.0, 37.3, 38.1, 38.3, 40.9, 58.0, 64.2, 68.8, 70.1, 70.4, 70.6, 76.4, 77.4, 82.7, 96.3, 122.3, 128.2, 130.3, 133.9, 138.1, 143.0, 156.9, 164.0, 165.7, 171.2, 172.7; HRMS calculated for $C_{42}H_{46}O_{14}F_3$ $[M+H]^+$ 831.2840, found 831.2859.

28-[(−)-α-Methoxy-α-(trifluoromethyl)phenylacetoxy]luminamicin (3). Previous procedure was performed with 1 (8.9 mg, 14.4 μmol), (−)-MTPA (10.1 mg, 43.2 μmol), EDCI (8.3 mg, 43.2 μmol), and DMAP (0.4 mg, 2.88 μmol) in CH_2Cl_2 (720 μl) to afford 3 (4.1 mg, 4.94 μmol, 34% yield) as a colorless solid: $[\alpha]_D^{26}$ +12.9 ° (c 0.185, $CHCl_3$); TLC R_f 0.63 (Benzene/Acetone 2/1); mp 115–116°C; IR (KBr) 3,521, 1,761, 1,178 cm^{-1}; ^{1}H-NMR (600 MHz, $CDCl_3$) δ 0.98 (3H, d, *J* = 6.9 Hz), 1.39 (1H, m), 1.43 (1H, m), 1.60 (3H, m), 1.70 (1H, dd, *J* = 13.2, 11.0 Hz), 1.77 (1H, m), 1.88 (1H, m), 2.17 (1H, m), 2.20 (1H, m), 2.46 (1H, m), 2.62 (1H, ddd, *J* = 15.1, 12.4, 2.7 Hz), 2.71 (1H, ddd, *J* = 14.9, 7.2, 2.7 Hz), 2.76 (1H, m), 2.90 (1H, ddd, *J* = 15.1, 7.2, 2.5 Hz), 3.27 (3H, s), 3.33 (1H, m), 3.35 (1H, m), 3.64 (1H, dd, *J* = 5.0, 1.9 Hz), 3.76 (1H, dd, *J* = 12.1, 4.7 Hz), 4.18 (1H, dd, *J* = 12.1, 2.2 Hz), 4.30 (2H, d, *J* = 3.9 Hz), 4.55 (1H, dd, *J* = 12.1, 1.7 Hz), 5.46 (1H, dd, *J* = 9.6, 2.5 Hz), 5.49 (1H, dd, *J* = 10.2, 5.5 Hz), 5.78 (1H, d, *J* = 13.5 Hz), 5.89 (1H, m), 5.89 (1H, m), 6.03 (1H, ddd, *J* = 10.2, 4.1, 3.9

Table 1. Vicinal coupling constants and torsinal constraints

Torsional angle	$^3J_{HH}$, Hz	Torsional constraints
H2-C2-C3-H3$_a$ (2.49 ppm)	12.4	180° ± 40°
H3$_a$ (2.49 ppm)-C3-C4-H4	1.9	−90° ± 40° or 90° ± 40°
H16-C16-C17-H17$_b$ (4.05 ppm)	<1.0	−90° ± 40° or 90° ± 40°
H16-C16-C17-H17$_a$ (4.87 ppm)	<1.0	−90° ± 40° or 90° ± 40°
H19$_b$ (2.46 ppm)-C19-C20-H20$_a$ (2.67 ppm)	2.2	−90° ± 40° or 90° ± 40°
H19$_b$ (2.46 ppm)-C19-C20-H20$_b$ (3.29 ppm)	12.6	180° ± 40°
H19$_a$ (2.86 ppm)-C19-C20-H20$_b$ (3.29 ppm)	2.0	−90° ± 40° or 90° ± 40°
H28-C28-C29-H29	10.7	180° ± 40°

Hz), 7.94 (1H, d, J = 13.5 Hz); ^{13}C-NMR (150 MHz, $CDCl_3$) δ 14.9, 16.0, 18.7, 27.9, 29.6, 32.9, 33.0, 37.0, 38.1, 38.3, 41.1, 58.0, 64.3, 68.9, 69.8, 70.5, 70.6, 76.4, 77.4, 82.8, 96.5, 122.5, 128.2, 130.3, 134.1, 138.0, 142.8, 156.8, 164.0, 165.7, 171.1, 172.8; HRMS calculated for $C_{42}H_{45}O_{14}F_3$ $[M]^+$ 830.2734, found 830.2761.

Results and Discussion

Distance and Dihedral Constraints Derived from NMR Experiments. Torsional constraints were obtained by applying the Karplus equation to vicinal proton–proton scalar coupling constants obtained by the 1D proton spectrum with high resolution (21). A proton–proton coupling constant >10 Hz was treated as indicating an anti H–H orientation and a dihedral-angle estimate of 180° ± 40°. A coupling constant <3 Hz was considered indicative of a *gauche* orientation, i.e., −90° ± 40° or 90° ± 40°. The resulting torsional constraints are given in Table 1.

To obtain distance constraints, 2D-TROESY spectra were measured with mixing times of 100, 150, 200, 250, and 300 ms. A plot of the volume of the cross-peak versus mixing time showed linearity up to 200 ms. Therefore, the proton–proton distance constraints were based on the integrated cross-peaks from the 200-ms spectrum. Fig. 7, which is published as supporting information on the PNAS web site, shows a part of the 2D-TROESY spectrum measured with a mixing time of 200 ms. Volumes of the five nonoverlapping geminal proton cross-peaks were averaged and used for calibrating measured ROE volumes. A distance of 1.8 Å was used as a distance reference for geminal proton cross-peaks. This calibration yielded the theoretically expected value, 2.4 Å, for the distance between H5 and H6. Distance constraints were classified into three categories corresponding to 1.8–2.7, 1.8–3.5, and 1.8–5.0 Å, corresponding to strong, medium, and weak ROEs, respectively. For the distance constraints related to methylene protons at C27 (H27$_{a,b}$), of which chemical shifts are overlapping, or methyl protons of 2-methoxy, 10-methyl, or 14-methyl groups, carbon atoms attached to these protons were used to estimate target distances. In such a case, 1.0 Å was added to the upper boundary of the constraints (22). For example, the strong ROE observed between H4 and the 14-methyl group is converted to a distance constraint between H4 and carbon atom of 14-methyl group (14MeC), the range of which is 1.8–3.7 Å. A total of 43 distance constraints were obtained as shown in Table 2.

Determination of Absolute Stereochemistry of Luminamicin. Table 3 lists the number of energetically possible conformers obtained from CAMDAS calculation for 32 different configurations. About 2,500~3500 distinct conformers were obtained for each configuration. Then, we calculated RMS deviations for all conformers generated by CAMDAS to determine which configurations can adopt conformers accommodating the distance and dihedral constraints. All distance constraints were treated with equal

Table 2. Distance constraints obtained by the 2D-TROESY experiments

Atom A	Atom B	The upper bound, Å	Atom A	Atom B	The upper bound, Å
H2	2MeC	3.7	H9	H15	5.0
H2	H3$_b$ (1.41 ppm)	2.7	H10	H11	3.5
H2	H4	2.7	H10	H15	3.5
H2	H5	3.5	10MeC	H11	3.7
2MeC	H25	4.5	H12	14MeC	3.7
2MeC	C27	5.5	14MeC	H16	3.7
H3$_b$ (1.41 ppm)	H4	3.5	14MeC	H29	3.7
H3$_b$ (1.41 ppm)	H5	2.7	H15	H16	3.5
H3$_a$ (2.49 ppm)	H4	3.5	H15	H17$_b$ (4.05 ppm)	2.7
H3$_a$ (2.49 ppm)	H15	2.7	H16	H17$_b$ (4.05 ppm)	2.7
H4	H5	2.7	H16	H17$_a$ (4.87 ppm)	2.7
H4	H12	3.5	H16	H28	5.0
H4	14MeC	3.7	H16	H29	2.7
H6	H7	2.7	H17$_a$ (4.87 ppm)	H28	2.7
H6	H8$_a$ (1.43 ppm)	3.5	H19$_b$ (2.46 ppm)	H20$_a$ (2.67 ppm)	2.7
H7	H8$_b$ (1.69 ppm)	2.7	H19$_a$ (2.86 ppm)	H20$_b$ (3.29 ppm)	2.7
H8$_a$ (1.43 ppm)	H9	2.7	H20$_b$ (3.29 ppm)	H25	2.7
H8$_b$ (1.69 ppm)	H9	2.7	H25	C27	3.7
H8$_b$ (1.69 ppm)	10MeC	3.7	H25	H28	2.7
H8$_b$ (1.69 ppm)	H11	3.5	C27	H29	3.7
H9	H10	2.7	H28	H29	3.5
H9	10MeC	3.7			

Table 3. RMS deviations of CAMDAS-generated conformers of luminamicin from experimentally determined values

Configuration with respect to the decalin ring							Configuration of C2, C16, C28, and C29				Smallest RMS deviation from exptl distance constraints, Å	RMS deviation from exptl dihedral constraints, °*	Number of conformers obtained by CAMDAS
C4	C7	C9	C10	C11	C12	C13	C2	C16	C28	C29			
R	S	S	S	S	R	R	R	R	R	R	0.34	0.0	3,185
R	S	S	S	S	R	R	R	R	R	S	0.32	0.9	2,369
R	S	S	S	S	R	R	R	R	S	R	0.00	0.0	3,287
R	S	S	S	S	R	R	R	R	S	S	0.17	18.6	2,749
R	S	S	S	S	R	R	R	S	R	R	0.36	18.5	3,022
R	S	S	S	S	R	R	R	S	R	S	0.27	0.0	2,769
R	S	S	S	S	R	R	R	S	S	R	0.33	19.0	3,016
R	S	S	S	S	R	R	R	S	S	S	0.33	9.5	2,931
R	S	S	S	S	R	R	S	R	R	R	0.39	37.2	3,294
R	S	S	S	S	R	R	S	R	R	S	0.51	0.0	3,064
R	S	S	S	S	R	R	S	R	S	R	0.36	8.1	3,375
R	S	S	S	S	R	R	S	R	S	S	0.38	18.7	3,235
R	S	S	S	S	R	R	S	S	R	R	0.41	19.2	2,954
R	S	S	S	S	R	R	S	S	R	S	0.19	0.0	3,392
R	S	S	S	S	R	R	S	S	S	R	0.43	20.0	2,895
R	S	S	S	S	R	R	S	S	S	S	0.17	0.2	3,298
S	R	R	R	R	S	S	R	R	R	R	0.52	11.4	3,297
S	R	R	R	R	S	S	R	R	R	S	0.54	14.3	3,160
S	R	R	R	R	S	S	R	R	S	R	0.43	0.0	3,477
S	R	R	R	R	S	S	R	R	S	S	0.27	36.5	3,105
S	R	R	R	R	S	S	R	S	R	R	0.38	0.0	3,109
S	R	R	R	R	S	S	R	S	R	S	0.36	8.1	3,321
S	R	R	R	R	S	S	R	S	S	R	0.49	13.8	3,067
S	R	R	R	R	S	S	R	S	S	S	0.53	8.9	3,252
S	R	R	R	R	S	S	S	R	R	R	0.39	0.0	2,806
S	R	R	R	R	S	S	S	R	R	S	0.33	19.0	2,955
S	R	R	R	R	S	S	S	R	S	R	0.35	0.0	2,909
S	R	R	R	R	S	S	S	R	S	S	0.36	18.5	2,886
S	R	R	R	R	S	S	S	S	R	R	0.17	18.7	2,569
S	R	R	R	R	S	S	S	S	R	S	0.00	0.0	3,204
S	R	R	R	R	S	S	S	S	S	R	0.50	18.9	2,521
S	R	R	R	R	S	S	S	S	S	S	0.37	0.0	3,329

*Calculated for the conformer having the smallest RMS deviations from the distance constraints.

weight, although they were classified as strong, medium, and weak. For constraints including nonoverlapping geminal protons (3-, 8-, 17-, 19-, or 20-methylene protons), careful analysis was done when estimating target dihedral angles and proton–proton distances. For example, $H3_a$ (2.49 ppm) is included in a total of four constraints, i.e., two dihedral constraints and two distance constraints as shown in Tables 1 and 2. The proton corresponding to $H3_a$ should simultaneously satisfy all of these four constraints. Because we cannot establish the stereospecific assignments on 3-methylene protons ($H3_a$ and $H3_b$) in advance, we first need to consider all combinations when estimating target dihedral angles or target proton–proton distances. For example, we first estimate a total of four dihedral angles, i.e., two dihedral angles are combination between H2 and two 3-methylene protons, and other two are combination between H4 and two 3-methylene protons. Then, we determine which of two 3-methelyne protons can simultaneously satisfy two dihedral constraints included in Table 1. The identified proton can be considered to correspond to $H3_a$ (2.49 ppm). Next, for the identified 3-methelyne proton, we estimate two target distances related to $H3_a$ (2.49 ppm) in Table 2. The similar procedure was also performed for the constraints on 8-, 17-, 19-, or 20-methylene protons. Table 3 includes the smallest RMS distance deviations obtained for each configuration. The conformers satisfying all experimental constraints were found in only two configurations. For luminamicin with the *R*, *S*, *S*, *S*, *S*, *R*, and *R* configurations at C4, C7, C9, C10, C11, C12, and C13, respectively, C2, C16, C28, and C29 should have the *R*, *R*, *S*, and *R* configurations, respectively. On the other hand, for luminamicin with the *S*, *R*, *R*, *R*, *R*, *S*, and *S* configurations at C4, C7, C9, C10, C11, C12, and C13, respectively, the results embodied the *S*, *S*, *R*, and *S* configurations at C2, C16, C28, and C29, respectively. Obviously, the former configuration is an enantiomer of the latter one. This means that NMR constraints could not distinguish between enantiomers. This was an expected result, because distance and dihedral constraints can provide only relative structural orientation. The final determi-

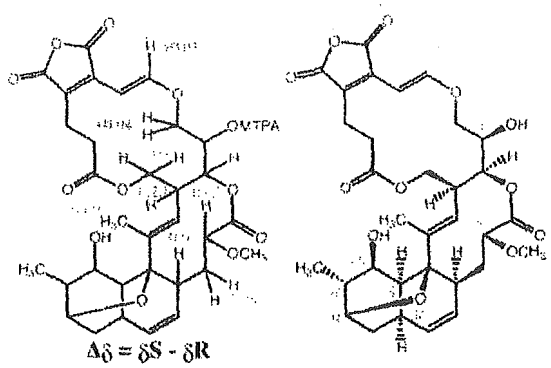

Fig. 3. Δδ Values of MTPA esters from luminamicin (1).

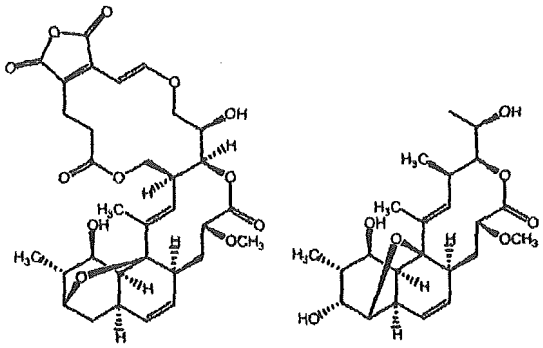

Luminamicin Nodusmicin

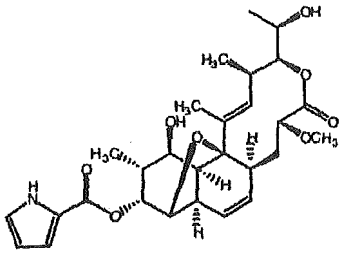

Nargenicin

Fig. 4. Structures of luminamicin, nodusmicin, and nargenicin.

nation of absolute stereostructure of luminamicin was done by using the result of the following modified Mosher method.

1 was treated with (*R*)-(+)- and (*S*)-(−)-2-methoxy-2-trifluoromethyl-2-phenylacetic acid (MTPA) in the presence of EDCI and DMAP to afford the (*R*)-(+)- and (*S*)-(−)-MTPA

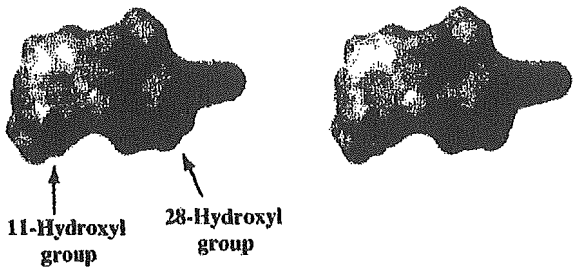

Fig. 6. Stereoview of surface representation of luminamicin. This view direction is the same as that of Fig. 5*B*.

esters (2 and 3) (see Scheme 1, which is published as supporting information on the PNAS web site). Fig. 3 shows the $\Delta\delta$ values (δ_S–δ_R) obtained from the ^{1}H-NMR data of 2 and 3, which are included in Table 4, which is published as supporting information on the PNAS web site. The $\Delta\delta$ values for H_3-14-Me, H-16, and H-29 were negative, whereas positive $\Delta\delta$ values were obtained for H-26 and H_2-27, thus indicating an *R* configuration. The absolute configurations therefore at C2, C4, C7, C9, C10, C11, C12, C13, C16, C28, and C29 of 1 were assigned as *S*, *S*, *R*, *R*, *R*, *R*, *S*, *S*, *S*, *R*, and *S*, respectively.

This configuration is the same as that found in nodusmicin (7) and nargenicin (8), which have a chemical structure quite similar with luminamicin (Fig. 4).

Description of the 3D Structure of Luminamicin. The process described above led to a set of two energy-minimized structures for luminamicin, which have Merck Molecular Force Field energies of 135.6 and 142.1 kcal/mol, respectively. Fig. 5 shows stereopairs of the best-fit superposition of the heavy atoms for these two structures. The structures only differ with respect to the orientation of the 2-methoxy group. As shown is Fig. 1, luminamicin consists of three different rings, i.e., a decalin, a

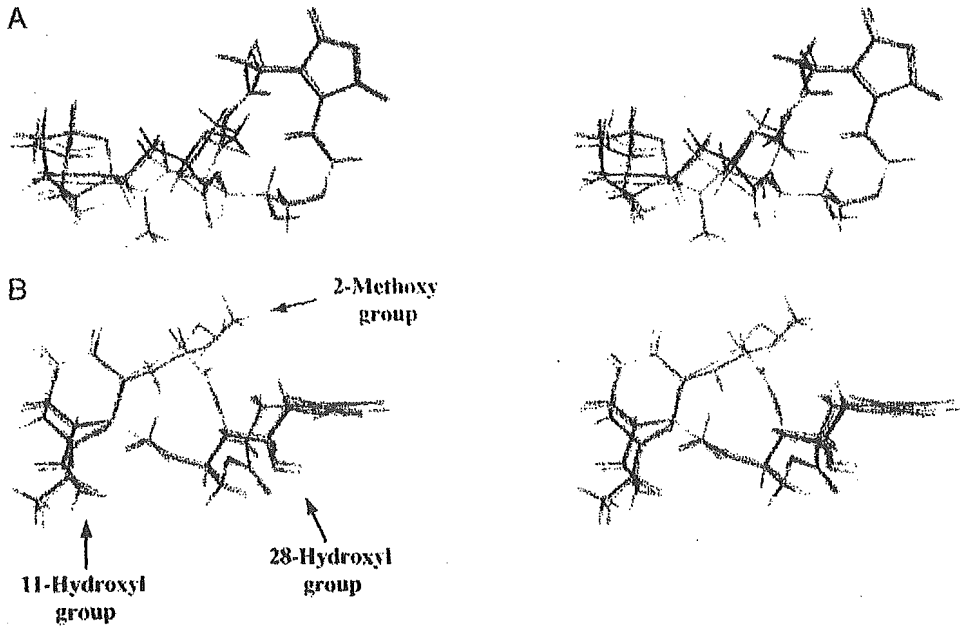

Fig. 5. Stereopairs of the superposition of the resulting two 3D structures of luminamicin. Black and green structures have Merck Molecular Force Field energies of 135.6 and 142.1 kcal/mol, respectively. These are the results of the best fit of the heavy atoms. *B* is rotated 90° in relation to *A*.

10-membered macrolactone, and a 14-membered macrolactone. The earlier NMR study described only the stereochemistry of the decalin ring (Fig. 2). Both C3 and C14 of the 10-membered macrolactone ring occupy equatorial positions relative to the decalin ring, as indicated in Fig. 2. The two strong ROEs between H4 and 14-methyl group and H12 and 14-methyl group conclusively established the spatial orientation of the 14-methyl group. It must be on the same side with H4 and H12 of the decalin ring. The configuration of C2 was well defined by the ROEs between H2 and H4, 2-methoxy group and $H27_{a,b}$, and 2-methoxy group and H25. These ROEs result in the 2-methoxy group oriented to the 14-membered macrolactone. The 10- and 14-membered macrolactones were clearly found to be cis-fused in this study, because critical strong ROEs were observed between H16 and H29, H16 and 14-methyl group, and H29 and 14-methyl group, indicating that these protons are on one side of the molecule. Both of $H17_a$ and $H17_b$ have *gauche* orientation relative to H16, because both correlations of 16H to $H17_a$ and $H17_b$ are strong in the TROESY spectrum. The small values of $J_{16,17a}$ (<1.0 Hz) and $J_{16,17b}$ (<1.0 Hz) are also consistent with these *gauche* orientations. The orientation of olefinic group (C25 and C26) was established by the strong correlations of H25 to $H20_b$ and H27 in the TROESY spectrum. H25 is oriented inside the molecule and H26 is turned outside. The stereochemistry of C28 was determined by the strong ROE between H25 and H28, resulting in the 28-hydroxyl group oriented outside the molecule. The resulting 3D structure of luminamicin shows an interesting feature that the maleic anhydride functionality in conjugation with olefinic group of the 14-membered macrolactone is nearly perpendicular to the plane of the decalin and 14-membered macrolactone rings, as shown in Fig. 5.

Luminamicin has two hydroxyl groups at C11 and C28, which are expected to react with (*R*)-MTPA or (*S*)-MTPA. However, it appears that these reagents can react with only the 28-hydroxyl group. With respect to this phenomenon, we have obtained some relevant information from the 3D structure of luminamicin. As shown in Fig. 6, two hydroxyl groups at C11 and C28 are placed on one side of luminamicin. In addition, the 28-hydroxyl group is more exposed to the solvent, because its solvent-accessible surface area (36.9 Å) is larger than that of the hydroxyl group at C11 (29.7 Å). Therefore, we can consider that the reagents appear to more easily react at C28, and the (*R*)-MTPA or (*S*)-MTPA ester group attached at C28 most likely hinder the reaction occurring at C11.

In conclusion, the absolute stereostructure of luminamicin, an anaerobic antibiotic, has been determined by using the conformational analysis via high-temperature MD, NMR spectroscopy, and the modified Mosher method. Luminamicin (**1**) could be a new lead for medicines to compare with vancomycin, which is used clinically in pseudomembranous colitis therapy.

This work was supported in part by the Ministry of Education, Science, Sports, and Culture of Japan; the Japan Keirin Association; the Grant of the 21st Century COE Program; and a Kitasato University Research Grant for Young Researchers (to T.S. and H.G.).

1. Ōmura, S., Iwai, Y., Naagawa, A., Iwata, R., Takahashi, Y., Shimizu, H. & Tanaka, H. (1983) *J. Antibiot.* **36**, 109–114.
2. Ōmura, S., Imamura, N., Oiwa, R., Kuga, H., Iwata, R., Masuma, R. & Iwai, Y. (1986) *J. Antibiot.* **39**, 1407–1412.
3. Ōmura, S., Iwata, R., Iwai, Y., Taga, S., Tanaka, Y. & Tomoda, H. (1985) *J. Antibiot.* **38**, 1322–1326.
4. Tomoda, T., Iwata, R., Takahashi, Y., Iwai, Y., Oiwa, R. & Ōmura, S. (1986) *J. Antibiot.* **39**, 1205–1210.
5. Hinda, M., Ui, H., Yamamoto, D., Monma, S., Iwai, Y., Sunazuka, T. & Ōmura, S. (2003) *Heterocycles* **59**, 497–500.
6. Rasmussen, R. R., Scherr, M. H., Whittern, D. N., Buko, A. M. & McAlpine, J. B. (1987) *J. Antibiot.* **40**, 1383–1393.
7. Whaley, H. A., Chidester, C. G., Mizsak, S. A. & Wnuk, R. J. (1980) *Tetrahedron Lett.* **21**, 3659–3662.
8. Celmer, W. D., Chmurny, G. N., Moppett, C. E., Ware, R. S., Watts, P. C. & Whipple, E. B. (1980) *J. Am. Chem. Soc.* **102**, 4203–4209.
9. Matsuzaki, K., Ikeda, H., Ogino, T., Matsumoto, A., Woodruff, H. B., Tanaka, H. & Ōmura, S. (1994) *J. Antibiot.* **47**, 1173–1174.
10. Matsuzaki, K., Ogino, T., Sunazuka, T., Tanaka, H. & Ōmura, S. (1997) *J. Antibiot.* **50**, 66–69.
11. Gouda, H., Matsuzaki, K., Tanaka, H., Hirono, S., Ōmura, S., McCauley, J. A., Sprengeler, P. A., Furst, G. T. & Smith, A. B. (1996) *J. Am. Chem. Soc.* **118**, 13087–13088.
12. Ohtani, I., Kusumi, T., Kashman, Y. & Kakisawa, H. (1991) *J. Org. Chem.* **56**, 1296–1298.
13. Dake, J. A., Dull, D. L. & Mosher, H. S. (1969) *J. Org. Chem.* **34**, 2543–2549.
14. Hwang, T.-L. & Shaka, A. J. (1992) *J. Am. Chem. Soc.* **114**, 3157–3159.
15. Hwang, T.-L. & Shaka, A. J. (1992) *J. Magn. Reson. B* **102**, 155–165.
16. States, D. J., Haberkorn, R. A. & Ruben, D. J. (1982) *J. Magn. Reson.* **48**, 286–292.
17. Tsujishita, H. & Hirono, S. (1997) *J. Comput. Aided Mol. Des.* **11**, 305–315.
18. Ryckaert, J.-P., Ciccotti, G. & Berendsen, H. J. C. (1977) *J. Comput. Chem.* **23**, 327–341.
19. Halgren, H. (1990) *J. Am. Chem. Soc.* **112**, 4710–4723.
20. de Haan, J. W. & van de Ven, L. J. M. (1973) *Org. Magn. Reson.* **5**, 147–153.
21. Karplus, M. (1963) *J. Am. Chem. Soc.* **85**, 2870–2871.
22. Steinmetz, W. E., Sadowsky, J. D., Rice, J. S., Roberts, J. J. & Bui, Y. K. (2001) *Magn. Reson. Chem.* **39**, 163–172.

Comparison of Consensus Scoring Strategies for Evaluating Computational Models of Protein−Ligand Complexes

Akifumi Oda,*,† Keiichi Tsuchida,† Tadakazu Takakura,† Noriyuki Yamaotsu,‡ and Shuichi Hirono‡

Discovery Laboratories, Toyama Chemical Co., Ltd., 2-4-1 Shimookui, Toyama 930-8508, Japan, and School of Pharmaceutical Sciences, Kitasato University, 5-9-1 Shirokane, Minato-ku, Tokyo 108-8641, Japan

Received July 12, 2005

Here, the comparisons of performance of nine consensus scoring strategies, in which multiple scoring functions were used simultaneously to evaluate candidate structures for a protein−ligand complex, in combination with nine scoring functions (FlexX score, GOLD score, PMF score, DOCK score, ChemScore, DrugScore, PLP, ScreenScore, and X-Score), were carried out. The systematic naming of consensus scoring strategies was also proposed. Our results demonstrate that choosing the most appropriate type of consensus score is essential for model selection in computational docking; although the vote-by-number strategy was an effective selection method, the number-by-number and rank-by-number strategies were more appropriate when computational tractability was taken into account. By incorporating these consensus scores into the FlexX program, reasonable complex models can be obtained more efficiently than those selected by independent FlexX scores. These strategies might also improve the scoring of other docking programs, and more-effective structure-based drug design should result from these improvements.

1. INTRODUCTION

Drug design that is based on the three-dimensional (3D) structures of biopolymers, which are candidate drug targets, is commonly referred to as structure-based drug design (SBDD). Predictions of the 3D structures of protein−ligand complexes play an important role in SBDD.[1−3] Over the past 15 years, a variety of computational docking programs that predict protein−ligand complex structures have been developed.[4−7] FlexX is one of the most useful docking programs,[4] in which ligand molecules are divided into small fragments and reconstructed in the active sites of target proteins guided by physicochemical interactions. It is widely used for computational docking trials.

Because docking programs generally produce numerous model candidates for one system, it is essential to evaluate the predicted models and determine which are the most suitable. Although free energy calculations of these systems are required for this purpose, accurate calculations of free energies using molecular simulations are very time-consuming. Therefore, various scoring functions that approximately estimate the binding free energies of protein−ligand systems using simple functions without molecular simulations have been developed.[4−13] Scoring functions can be classified into three groups: empirical, knowledge-based, and force-field-based scoring functions.[3,14] Empirical scoring functions are fit to reproduce experimental data, such as experimentally obtained binding energies and conformations, as a sum of several parametrized functions and are the most widely employed. Knowledge-based scoring functions are derived from experimental structures and are represented by relatively simple atomic interaction-pair potentials. Force-field-based scoring functions are derived from molecular mechanics force-fields and are represented by physicochemical-interaction terms, such as van der Waals potentials and Coulombic interactions. These scoring functions rank the complex structure candidates, and the most highly ranked models are adopted.

As well as their role in model selection, scoring functions have three essential functions in the computational docking process.[1,15] First, during the steps of model construction, the scores of the docking models that are under construction are calculated using scoring functions. The obtained values are then utilized in the next construction step. Thus, scoring functions are required not only in the selection of constructed models but also in the model-construction steps themselves. Second, one or a few predicted models are selected from a large number of model candidates using scoring functions (as mentioned above). Third, in virtual screening trials, in which numerous ligands are docked into one target protein, scoring functions can identify those that potentially represent favorable drug candidates. These three roles are all important for SBDD.

Scoring functions play significant roles in SBDD, and various functions have been proposed. However, building a scoring function that can make use of every protein−ligand system remains the "final frontier" of computational docking studies.[16] Every existing scoring function has specific advantages and disadvantages, and there is no de facto standard. Although this might suggest that different scoring functions are required for different protein−ligand systems, discussions about which scoring function is most suitable for a particular system are often difficult when the complex structures are not experimentally observed. Recently, the concept of a consensus score was proposed for model selection in computational docking and virtual screening

* Corresponding author phone: +81 76 431 8218; fax: +81 76 431 8208; e-mail: AKIFUMI_ODA@toyama-chemical.co.jp.
† Toyama Chemical Co., Ltd.
‡ Kitasato University.

10.1021/ci050283k CCC: $33.50
Published on Web 11/24/2005

Table 1. Consensus Scores

	consensus scoring method according to ref 19[a]	
threshold	rank-by-number	rank-by-rank
number-by	number-by-number	number-by-rank
rank-by	rank-by-number	rank-by-rank
percent-by	percent-by-number	percent-by-rank

[a] Note that the names of the consensus scoring strategies in the current study differ from those given in ref 19.

for model selections with three types of selection criteria: in the first, models with consensus score values that are less than or equal to $x_{threshold}$ are selected; in the second, the models are ranked according to the consensus scores and the top $y_{threshold}$ models are selected; in the third, the top $z_{threshold}$ percent candidates are selected. No systematic studies of these three criteria have been reported previously. Hence, in the present study, we compared these criteria for both rank-by-number and rank-by-rank consensus scores. A total of six types of average-based consensus score were compared in terms of their effectiveness for model selection. The first criterion, under which the consensus score values themselves are used for model selection, was denoted using the prefix "number-by-" in this study, whereas the second and third criteria were indicated by the prefixes "rank-by-" and "percent-by-", respectively. Because names such as number-by-rank-by-number (referring to the rank-by-number consensus score with the number-by criterion) were considered to be too long, we chose to describe this type of consensus scoring strategy as number-by-number. In the same way, the terms number-by-rank, rank-by-number, rank-by-rank, percent-by-number, and percent-by-rank were used. Note that the meanings of rank-by-number and rank-by-rank in this study differ from those employed in ref 19. The AASS corresponded to the number-by-number, rank-by-number, and percent-by-number approaches.[30] The six types of average-based consensus score are shown in Table 1. In this study, autoscaled scores are used for the by-number strategies. Optimizations of the thresholds, $x_{threshold}$, $y_{threshold}$, and $z_{threshold}$, were also carried out.

By contrast, the rank-by-vote approach uses a majority-vote-based consensus score. According to this strategy, if the score value of a model meets the standard that is set for a vote, the model is awarded one vote. This procedure is repeated for all of the scoring functions that are included in the consensus score, and the models that have many votes are eventually selected. Some previous studies[17-20] employed the rule that "models whose scores are within the top $z_{threshold}$ percent win one vote", and the rule that "models whose scores are less than, or equal to, $x_{threshold}$ win one vote" was used in CScore.[21] In addition to these criteria, the idea that the "top $y_{threshold}$ models obtain one vote" could also be applied. No previous comparative studies have examined these three standards, and they have all been referred to using the same term—rank-by-vote. In the current study, we proposed different names for these three approaches: the majority-vote-based consensus scoring strategy that awarded votes to "models whose scores are within the top $z_{threshold}$ percent" was referred to as vote-by-percent, the strategy that awarded votes to "models whose scores are less than, or equal to, $x_{threshold}$" was referred to as vote-by-number, and the consensus scoring strategy in which the "top $y_{threshold}$ models" were awarded votes was referred to as vote-by-rank. Thus, the rank-by-vote strategy described in ref 19 was referred to as the vote-by-percent strategy in the current study, and the CScore strategy was referred to as the vote-by-number strategy. In the present study, these three types of majority-vote-based consensus scores were investigated together with six types of average-based consensus score. In contrast to the average-based consensus scores, in which only one threshold is used, the vote-by strategies require two types of threshold: one for the voting standard and another for the number of votes. For example, in the vote-by-percent strategy, the model candidate with a score within the top $z_{threshold}$ percent obtains one vote for one scoring function (the $z_{threshold}$ is the threshold for the voting standard), and a candidate with a total number of votes for all of the scoring functions that is greater than, or equal to, the $w_{threshold}$ will eventually be selected (the $w_{threshold}$ is the threshold for the number of votes). Figure 3 illustrates the vote-by strategy. Both thresholds of the vote-by strategies were optimized in our study.

2.5. Evaluations of Consensus Scores. To evaluate the consensus scores, we initially determined the thresholds that enabled reasonable solutions to be obtained for all of the systems without exception. Using these thresholds, the number of model candidates could be reduced, and we investigated how many remained in each candidate group. For example, in the number-by strategies, the $x_{threshold}$ values were optimized in order to reduce the number of models as much as possible while at least one reasonable model remained in the filtered sets of candidates, the consensus score values of which were less than, or equal to, the $x_{threshold}$ for all 220 protein−ligand systems without exceptions. Similarly, the $y_{threshold}$ and $z_{threshold}$ values were optimized for the rank-by and percent-by strategies, respectively. These thresholds are illustrated in Figure 4. As shown in the figure, the model with the best score from all of the reasonable models was identified, and its score value, rank, and percentage were investigated. These values were obtained for all 220 protein−ligand systems, and the highest values

Model	A score	B score	C score		Number of votes		Elected or excluded
1	0.525	0.564	0.671		0		excluded
2	**0.434**	**0.000**	0.911		2		**elected**
3	**0.000**	**0.232**	**0.000**	vote $x_{threshold} = 0.5$	3	selection $w_{threshold} = 2$	**elected**
4	1.000	1.000	1.000		0		excluded
5	0.566	0.777	0.620		0		excluded
6	**0.303**	**0.412**	**0.405**		3		**elected**

Figure 3. Vote-by strategies.

Model	RMSD	Score
A	3.442	0.100
B	5.260	0.200
C	1.952	0.300
D	0.085	0.400
E	6.435	0.500

$x_{threshold} = 0.300$
$y_{threshold} = 3$
$z_{threshold} = 60\%$

Figure 4. Thresholds. The solution with a RMSD ≤ 2.0 Å was selected as a focus, and its score value ($x_{threshold}$), rank order ($y_{threshold}$), and top % ($z_{threshold}$) were adopted as the thresholds.

among the 220 scores, ranks, and percentages were set as the $x_{threshold}$, $y_{threshold}$, and $z_{threshold}$ values, respectively. Using these thresholds, at least one reasonable model could be obtained for all 220 systems. In contrast to average-based consensus scores, not only $x_{threshold}$, $y_{threshold}$, $z_{threshold}$ but also $w_{threshold}$ need to be optimized for majority-vote-based strategies. When the thresholds for voting standards ($x_{threshold}$, $y_{threshold}$, or $z_{threshold}$) were defined, each model obtained a certain number of votes by vote-by strategies. For example, the situation in which model 1 wins three votes, model 2 wins one vote, and model 3 wins five votes and only models 1 and 2 are "reasonable models", is considered. For this situation, the appropriate $w_{threshold}$ is three, because when the $w_{threshold}$ is greater than three, no reasonable models are selected. When $w_{threshold}$ is less than three, it is possible to select reasonable models, but a higher threshold is more appropriate. In this way, an appropriate $w_{threshold}$ was investigated for each vote-by strategy and each $x_{threshold}$, $y_{threshold}$, and $z_{threshold}$. The ratio of the remaining models to all of the candidates was referred to as the compression ratio and was calculated using the following formula:

$$p_{compress} = \sum_{220\ systems} n_{remain} / \sum_{220\ systems} n_{all} \qquad (3)$$

Here, $p_{compress}$ is the compression ratio, n_{remain} is the number of remaining models using the threshold, and n_{all} is the total number of models. The compression ratio was used as an indicator of the ability of each consensus score strategy.

Using conditions under which reasonable models could be obtained for all 220 systems without exception, the compression ratio was generally relatively large (that is, not well-compressed). Therefore, the numbers of protein−ligand systems for which reasonable models could be selected using several predefined threshold values were also elucidated, to investigate the scenario in which reasonable models could be obtained, not for all 220 systems, but for the majority of the systems, with few exceptions. Using these predefined thresholds, a good compression ratio was expected at the expense of the accuracy of the modeling of a few of the protein−ligand systems. For this investigation, not only the compression ratio but also the ratio of accurate modeling (that is, the ratio of accurately modeled systems to the total number of systems) was evaluated using the following formula:

$$p_{accurate} = n_{accurate}/n_{all} \qquad (4)$$

Here, $p_{accurate}$ is the ratio of accurate modeling, $n_{accurate}$ is the number of protein−ligand systems in which reasonable models can be obtained using the predefined threshold, and n_{all} is the total number of systems (in this study, $n_{all} = 220$ for the complete test set, $n_{all} = 57$ for those complexes with high-affinity ligands only, and $n_{all} = 122$ for groups including complexes with $n \geq 250$). The tradeoff between accuracy and efficiency was investigated using the $p_{compress}$ and $p_{accurate}$ values for each consensus score.

In the current study, the combinations of scoring functions with the best $p_{accurate}$ and $p_{compress}$ values were investigated for each strategy and threshold. However, the computational cost of evaluating all 511 combinations would have been extremely high. Therefore, from a practical standpoint, the results produced using all nine functions could be discussed for the simple consensus scoring methods without exploring the combinations; thus, the computational cost that was involved in searching for the best combination was reduced. To further simplify the procedure, we also investigated the consensus scores using only five of the scoring functions: FlexX score, GOLD score, PMF score, DOCK score, and ChemScore. These functions were included in the CScore module of the SYBYL 6.9 program. Because all of these scores could be calculated simultaneously in a single CScore trial, using the consensus scores with these five functions was the simplest method for our study. Not only exhaustive investigations of 511 combinations but also tests of these simplified consensus scores were carried out in this study.

Consensus scores for the experimental structures of protein−ligand complexes were also calculated in order to consider the wider applications of the consensus scoring strategies. As the experimental structures were regarded as the "correct" answers, the consensus scores for these structures were expected to reflect the ability of the scoring strategies in applications with real complexes. The number-by-number strategy was used for this purpose, because it was one of the most useful consensus scoring strategies and could easily be compared among different protein−ligand complex systems. The models that were calculated by FlexX were used as parent populations for the consensus scoring. The experimental structure was added to n models obtained by FlexX, so the parent population for the consensus scoring included $n + 1$ models.

The ranks and percentages of models might be biased by differences of the numbers of model candidates between test complexes. For example, although we considered that the "top three models of six candidates" means the same as the "top three models of 500 candidates" in rank-by strategies, the latter three models appeared to be more highly selected than the former models. Because the flexibilities of ligands and the sizes of active sites were very different from each other for 220 test systems, it is not a practical setting that FlexX generates completely the same number of candidates for all systems. Thus, we extracted the 122 complex systems that have more than or equal to 250 candidates, and we compared the abilities of consensus scoring strategies for these 122 systems. By using this test set, the bias caused by differences of the numbers of candidates was reduced, and the dependencies of abilities of consensus scores on n were investigated.

3. RESULTS AND DISCUSSION

3.1. Selection of Reasonable Models for the 220 Protein−Ligand Systems. To determine the thresholds under which at least one reasonable model could be selected

Table 2. Comparison of the Nine Types of Consensus Score

(a) Number-by, Rank-by, and Percent-by Strategies

	threshold	$p_{compress}$ of best combination
number-by-number	$x_{threshold} = 0.452$	0.399
number-by-rank	$x_{threshold} = 151$	0.519
rank-by-number	$y_{threshold} = 151$	0.519
rank-by-rank	$y_{threshold} = 151$	0.519
percent-by-number	$z_{threshold} = 62.0\%$	0.617
percent-by-rank	$z_{threshold} = 62.4\%$	0.623

(b) Vote-by Strategies

	threshold for vote or not	threshold for number of votes ($w_{threshold}$)/number of functions included in best combination	$p_{compress}$ of best combination
vote-by-number	$x_{threshold} = 0.5$	5 votes/7 voters	0.371
vote-by-rank	$y_{threshold} = 150$	2 votes/3 voters	0.510
vote-by-percent	$z_{threshold} = 70\%$	3 votes/3 voters	0.502

for all 220 protein−ligand systems without exception, nine consensus scoring strategies and 511 combinations of scoring functions (that is, a total of 4599 types of consensus scores) were examined. The compression ratios that were produced using these thresholds were also investigated, that is, the compression ratios under the condition $p_{accurate} = 1.0$. Although all 511 combinations for each strategy were systematically evaluated, the combination that gave the best (smallest) compression ratio is focused on here (this was defined as the "best combination"). The best combinations are summarized in Table 2, in which both the thresholds and the compression ratios are described. For example, in the case of the number-by-number strategy, the best combination included the FlexX score, GOLD score, PMF score, DOCK score, PLP, and ScreenScore (as shown in Table S2 of the Supporting Information, and see below for discussion). After the autoscaling of the six scores, the average value—that is, the number-by-number consensus score—was calculated for each model. The $x_{threshold}$ of this combination for the number-by-number strategy was 0.452, which meant that at least one reasonable model was produced for each of the 220 protein−ligand systems by selecting the models with number-by-number consensus scores that were less than, or equal to, 0.452 (Table 2a). Using this strategy and threshold value, the number of model candidates to be explored was expected to be reduced to about 40% of the current size, because the compression ratio was equal to 0.399 (Table 2a). The vote-by-number strategy gave the best compression ratio for selecting suitable models for all 220 systems (Table 2a). In the best combination of vote-by-number, when the auto scaled value of one score was less than, or equal to, 0.5 for one model, it obtained one vote because $x_{threshold} = 0.5$ (Table 2b). When one model received more than, or equal to, five votes from the seven voters, it was selected because $w_{threshold} = 5$. Although the vote-by-percent strategy has been discussed for use in virtual screening trials in some previous reports,[17−20] our result suggests that a vote-by-number strategy, such as CScore, is a more appropriate majority-vote-based consensus score system for model selections. The second-best was the number-by-number strategy, which gave the best compression ratio of all average-based consensus scores.

The combinations that gave the top 10 compression ratios for all nine consensus scoring strategies are shown in Table S2 of the Supporting Information. As shown in Table S2a and g, for number-by-number and vote-by-number strategies, which had compression ratios that were superior to those of the other approaches, FlexX score, PLP, and ScreenScore were included in many of the top 10 consensus scores. It has been reported previously that these scoring functions work well when they are used independently.[20,22] Our results suggest that they are appropriate not only for independent scoring but also for consensus scoring. However, although it was reported that the GOLD score and DOCK score implemented in the CScore module were less successful when used alone, they appear high up in the lists of successful consensus scoring methods shown in Table S2a and g (Supporting Information). These force-field-based scoring functions are based on a different concept from that used to develop the empirical and knowledge-based scoring functions, and they seem to compensate for the shortcomings of the empirical scoring functions (such as FlexX score, PLP, and ScreenScore). By contrast, ChemScore and X-Score appeared in relatively few of the top 10 combinations. These are both empirical scoring functions, which are similar in form to FlexX score and ScreenScore, so mutual complementarity between them might not be expected. Therefore, ChemScore and X-Score do not seem to be appropriate for use together with FlexX score or ScreenScore, although they might perform well independently.

3.2. Efficient Selection of Reasonable Models with Some Exceptions. The investigations of the abilities of consensus scores discussed in the previous section were carried out under conditions in which reasonable models were selected for all protein−ligand test sets without exception (that is, $p_{accurate} = 1.0$). In this scenario, the values of the compression ratios tend to become overly large, because the thresholds are set to a high value if there are only a few systems for which reasonable models are difficult to search; this impairs the effectiveness of the consensus scores, even if they work well for most protein−ligand systems. In fact, the compression ratio was around 40%, even for the vote-by-number strategy, which was the best approach for this purpose. Therefore, the tradeoff between the $p_{accurate}$ and $p_{compress}$ values was investigated using several threshold values in order to make effective selections of reasonable models for as many protein−ligand systems as possible. In the current section, we discuss number-by, rank-by, and percent-by strategies, in which only one threshold is used. In the following section, consensus scores that are easy to use without exploring the combinations of scoring functions are described, and the tradeoff between the $p_{accurate}$ and $p_{compress}$ values is also discussed for vote-by strategies, in which two types of thresholds (that is, thresholds for the voting standard and for the number of votes) are required.

Figure S1 of the Supporting Information shows the ratios of the accurate modeling ($p_{accurate}$) for the number-by, rank-by, and percent-by strategies using several threshold values. In this section, the combination with the best $p_{accurate}$ among all of the 511 combinations is defined as the "best combination". The best combination for each threshold is summarized in Figure S1. Note that the meaning of best combination in this section is different from that in the previous section (where the term referred to the best compression ratio, rather than the best ratio of accurate modeling). The best combination of scoring functions for each threshold is shown in Table S3 of the Supporting Information together with the $p_{accurate}$

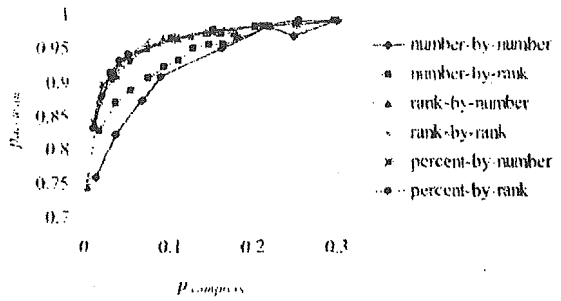

Figure 5. Compression ratios versus the ratios of accurate modeling when several threshold values were used.

and $p_{compress}$ values. In the rank-by and percent-by strategies, the behaviors of the by-number and by-rank consensus scores depending on the thresholds were similar to one another (Figures S1c and d). This indicates that, for these strategies, the results do not depend on whether by-number or by-rank approaches are used when the same thresholds are adopted.

Although Figure S1 (Supporting Information) illustrates the dependency of the $p_{accurate}$ values on thresholds, the tradeoff between the $p_{accurate}$ and $p_{compress}$ values cannot be discussed on the basis of this figure. Thus, the relationships between these parameters are explored in Figure 5, on the basis of the $p_{accurate}$ and $p_{compress}$ values presented in Table S3 (Supporting Information). Figure 5 shows that the $p_{compress}$ values of both of the number-by strategies were much worse than those of the rank-by and percent-by strategies when they were compared at the same values of $p_{accurate}$. This suggests that the rank-by and percent-by strategies are more appropriate for the effective selection of model candidates than the number-by strategies, which differs from the result we obtained for model selection with $p_{accurate} = 1.0$ (in which the number-by-number strategy was more appropriate). Therefore, different strategies should be adopted for different purposes, for example, "$p_{accurate} = 1.0$ is indispensable" or "a good balance between $p_{accurate}$ and $p_{compress}$ is desired".

For the number-by-number and rank-by-number strategies, the top 10 combinations of scoring functions in terms of $p_{accurate}$ are shown in Table 3. The $x_{threshold}$ and $y_{threshold}$ values were as small as possible while maintaining $p_{accurate} \geq 0.9$ for the best combinations (the top 10 combinations for the other strategies are shown in Table S4 in the Supporting Information). Table 3 demonstrates that while all of the top 10 combinations (excluding the number 1 combination) included more than, or equal to, four scoring functions in the rank-by-number strategy, all of the top 10 combinations in the number-by-number strategy included less than, or equal to, three functions; in particular, four of the top 10 combinations included only one scoring function and, thus, were not consensus scoring approaches. This suggests that the concept of consensus scoring does not work well for the number-by-number strategy, in contrast to the rank-by-number strategy, for the purpose of highly effective model selection at the expense of the accurate modeling of a few exceptional systems.

For the fast selection of model candidates, only the top model is frequently investigated. This is the situation with $y_{threshold} = 1$ for rank-by strategies. In Figure 6, the $p_{accurate}$ values of rank-by-rank and rank-by-number with $y_{threshold} = 1$ are illustrated. The results of independent scoring by nine

Table 3. Combinations of Scores That Gave the Top 10 Ratios of Accurate Modeling When $x_{threshold}$ and $y_{threshold}$ Were Small

(a) Number-by-Number ($x_{threshold} = 0.2$)

	scoring functions										
	F	G	PM	DO	C	Dr	PL	S	X	$p_{accurate}$	$p_{compress}$
1						√	√	√		0.9091	0.0882
2							√	√		0.9091	0.0957
3								√		0.9091	0.1179
4							√			0.9045	0.1183
5						√				0.9045	0.1186
6						√	√			0.9000	0.1050
7						√		√		0.8955	0.0909
8							√	√	√	0.8818	0.0706
9	√						√	√		0.8818	0.0856
10									√	0.8818	0.1099

(b) Rank-by-Number ($y_{threshold} = 10$)

	scoring functions										
	F	G	PM	DO	C	Dr	PL	S	X	$p_{accurate}$	$p_{compress}$
1					√		√			0.9091	0.0372
2	√	√		√	√	√	√			0.9045	0.0371
2	√	√		√		√		√		0.9045	0.0371
2					√	√	√	√		0.9045	0.0371
2	√	√		√	√	√	√	√		0.9045	0.0371
2	√	√			√	√	√			0.9045	0.0371
2	√	√		√		√	√	√		0.9045	0.0371
2		√			√	√	√		√	0.9045	0.0371
2		√			√	√	√	√	√	0.9045	0.0371
10					√		√	√	√	0.9045	0.0372

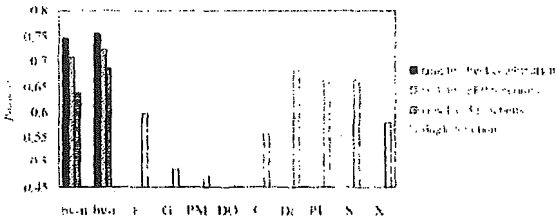

Figure 6. Ratios of accurate modeling for rank-by-number, rank-by-rank, and nine independent scoring functions when $y_{threshold} = 1$ was used. The "by-n" and "by-r" mean rank-by-number and rank-by-rank, respectively.

scores are also shown in the figure. For rank-by-number and rank-by-rank, not only the results of the best combination but also those of combinations including all nine functions and five CScore functions, that is, FlexX score, GOLD score, PMF score, DOCK score, and ChemScore, are illustrated. As shown in this figure, $p_{accurate}$ is around 0.75 for two types of rank-by strategies, and they were superior to all nine independent scoring functions. The $p_{accurate}$ values of the best combinations of two rank-by strategies were similar to one another, and this result was consistent with those of $y_{threshold} > 1$. However, for the combinations including all nine functions and five CScore functions, the results of rank-by-rank were better than those of rank-by-number. In fact, for rank-by-number, although the best combination and the combination including all nine functions were superior to all independent scoring functions, the result of the combination including five CScore functions was worse than the results of the independent scoring of DrugScore, PLP, and ScreenScore. On the other hand, for rank-by-rank, $p_{accurate}$ values obtained by not only best combination and the combination including all nine functions but also the combination including five CScore functions were better than

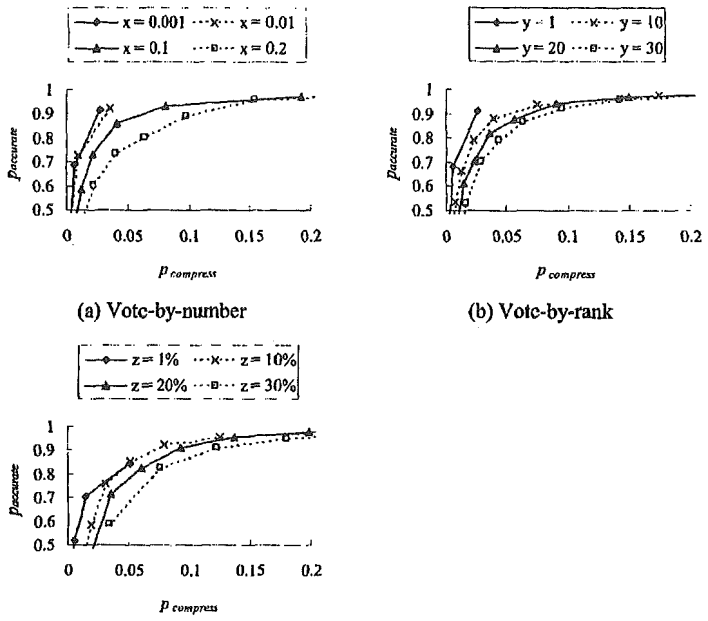

(a) Vote-by-number (b) Vote-by-rank

(c) Vote-by-percent

Figure 7. Results obtained using all nine functions depending on the thresholds.

those of all independent scoring functions. These results suggest that rank-by-rank is more robust in terms of combination of scoring functions than rank-by-number when $y_{threshold} = 1$.

3.3. Easy-to-Use Consensus Scores without Exploring the Combinations of Scoring Functions. For practical applications of consensus scores, exploring the best combination of scoring functions is highly expensive in terms of computational cost. Although thorough investigations of the combinations are desirable to allow detailed discussions, the computational cost is frequently as important as accuracy in drug design trials. Thus, in this section, consensus scores that are accurate and easy to use without the need to exhaustively explore the best combinations are discussed. One of these systems includes all nine functions and another includes the five CScore functions. In particular, the latter can be calculated using only a single CScore trial and is, therefore, the most simple consensus score considered in this study.

A comparison of the $p_{compress}$ values of the nine consensus scoring strategies under the condition $p_{accurate} = 1.0$ was carried out. The results are shown in Figure S2 of the Supporting Information, and they were similar to those of the best combinations mentioned in Section 3.1. These results support the finding that the two strategies, that is, vote-by-number and number-by-number, are appropriate for model selection of all systems without exception. Furthermore, for these two strategies, the $p_{compress}$ values calculated by both the combinations including all nine functions and five CScore functions were not much worse than those of the best combination. It suggests that these strategies also have advantages in terms of robustness of the combination of scoring functions.

The $p_{accurate}$ values obtained by the number-by, rank-by, and percent-by strategies depending on the thresholds are shown in Figure S3 of the Supporting Information (this is similar to the investigations mentioned in Section 3.2). The $p_{accurate}$ values of the rank-by and percent-by strategies using all nine functions or the five CScore functions were not much worse than those of the best combinations, in contrast to the number-by strategies. This means that, for the rank-by and percent-by strategies, the combinations using all nine functions or the five CScore functions, without exploring the best combinations, were effective in saving computational costs. Although the $p_{accurate}$ values of the rank-by-number and rank-by-rank strategies were similar to each other by using the best combinations, the rank-by-number strategy gave better $p_{accurate}$ values than the rank-by-rank strategy using all nine functions and the five CScore functions when $y_{threshold}$ was between 5 and 20. These results were different from those of $y_{threshold} = 1$, mentioned in Section 3.2, in which rank-by-rank was more robust than rank-by-number in terms of combinations of scoring functions.

In addition to the number-by, rank-by, and percent-by consensus scoring strategies, the dependencies of the $p_{accurate}$ and $p_{compress}$ values on the $w_{threshold}$ (the thresholds for the number of votes) were discussed for the vote-by strategies with the combinations including all nine functions. These discussions are useful for model selection by vote-by strategies with good balances between the $p_{accurate}$ and $p_{compress}$ values.

Figure 7 compares the balances between the $p_{accurate}$ and $p_{compress}$ values depending on the thresholds for the vote-by consensus scores including all nine functions, to determine which of the threshold values for the voting standard ($x_{threshold}$, $y_{threshold}$, and $z_{threshold}$) are desirable. For each of the thresholds for the voting standard, the threshold values for the number of votes ($w_{threshold}$) were set from 1 to 9. Figure 7 illustrates the results depending on both of the two thresholds (the complete data are shown in Table S5 in the Supporting